Merits and limits of a variational definition of the effective toughness of heterogeneous materials

Jean-Claude Michel, Pierre Suquet

Merits and limits of a variational definition of the effective toughness of heterogeneous materials

Jean-Claude Michel[1], Pierre Suquet[1]

Aix Marseille Univ, CNRS, Centrale Marseille
Laboratoire de Mécanique et d'Acoustique,
4 impasse Nikola Tesla, CS 40006, 13453 Marseille Cedex 13, France. [1]

Abstract

The objective of this study is to assess the variational definition of the effective fracture energy of a heterogeneous brittle material recently proposed by Schneider (*Int. J. Numer. Meth. Engng*, 2020) based on available mathematical homogenization results. First, similarities between the variational problems defining this effective surface energy and variational limit loads problems, are highlighted. These analogies allow us to compute the effective surface energy using the analytical and computational tools developed to determine the extremal surfaces of ideally plastic heterogeneous materials. Second, the same analogy opens the way to the derivation of variational bounds on the effective surface energy which appear to be in good agreement with the numerical simulations of other authors (Lebihain *et al*, *J. Mech. Phys. Solids*, 2021). Third, the status of this effective surface energy with respect to the effective toughness of heterogeneous materials is discussed. It is shown to always be a lower bound to the actual energy dissipated along the propagation of a crack in a heterogeneous material. Examples where both energies are different are exhibited.

1 Introduction

Toughening a brittle material by adding a second phase is a common practice in materials science. The role of this additional phase is to activate dissipative mechanisms at small scale, which are dormant in the original material, such as micro-plasticity, micro-cracking, debonding, slippage along particles, phase transformation (among others), whose role is to enhance the energy dissipated along the propagation of a crack.

From a fundamental point of view, it is interesting to deal with simpler problems and to investigate which contribution to the overall toughness can be expected from each individual mechanism. The question naturally arises of what is the contribution of the

[1]Corresponding author: suquet@lma.cnrs-mrs.fr

toughness of the individual constituents to the overall toughness. Therefore the question addressed in the present study is the following one: given an elastic-brittle composite (or heterogeneous) material with a known microstructure and knowing the elastic moduli and the fracture energy of each constituent, can an effective fracture energy be defined for the composite and how does it depend on the elastic moduli, toughness, volume fraction of the phases?

The topic of the effective toughness of a composite material considering the brittleness of its constituents as the only dissipative mechanism has been addressed in a number of studies over the last twenty years with an increasing interest in recent years. We will not review them in detail, referring the reader to the introductory sections in Ernesti and Schneider [17, 18], limiting ourself to a reminder of the points which are essential for our purpose.

First of all it is useful to recall that the problem of the failure of a solid material, even homogeneous, may be approached in different ways. In his celebrated 1920 article, Griffith envisioned the propagation of a crack as the creation of an additional surface resulting in an increase in the potential energy of the solid through a surface energy term. This idea, which may seem questionable if one considers with Griffith that this surface energy has the same status as the elastic energy and is therefore reversible, has nevertheless proved to be extremely fruitful and has given rise to various extensions. The most noticeable outcome is the notion of energy release rate (ERR) which follows directly from Griffith's energy balance. The crack advances when the ERR reaches a critical value G_c that we will call "fracture energy" of the material. Irwin noticed that fracture is a dissipative phenomenon and G_c is associated with a dissipation accompanying the propagation of the crack. The second deep influence of Griffith's work was that it inspired modern models of fracture and in particular the variational model of Francfort and Marigo [19] and its developments ([6] for a review).

In another pioneering work published in 1957, Irwin quantified the notion of stress singularity through the introduction of the stress intensity factors (SIF) in a linear elastic material. The SIF's soon became the cornerstone of the Linear Elastic Fracture Mechanics (LEFM). An opening crack propagates when the stress intensity factor reaches a critical value K_c, the "toughness" of the material (by an abuse of vocabulary, the word "toughness" sometimes refers in the literature to G_c, for which we will use the wording "fracture energy").

Although the two approaches (energy balance and stress singularity) have different roots, they largely overlap, at least for linear elastic materials, and the two critical notions G_c and K_c can be related in isotropic media by Irwin's relation $G_c = \frac{1-\nu^2}{E} K_c^2$ (mode I, plane strains).

In a pioneering work, Gao and Rice [22], using the stress intensity factor approach, computed the perturbation in the stress intensity factor K_I along the crack front caused by obstacles encountered by a crack with an initially straight front. The matrix material and the inclusions have the same elasticity, but their toughness differ. This stress intensity factor is a field varying along the crack front and Gao and Rice established an integral equation for this field at first order with respect to the geometric perturbation of the front. In their analysis the crack is forced to remain planar and its front, trapped by the inclusions, can only bend under an increasing applied load. Their study was later extended beyond first order, in particular by Bower and Ortiz [7] with experimental confirmations by Mower and Argon [39]. Roux *et al* [43] used Gao and Rice's perturbation analysis to propose a self-consistent definition of the effective toughness, distinguishing two regimes corresponding respectively to a weak contrast between the toughnesses of the phases allowing the crack to cross the inclusions (particle-crossing or "weak pinning" regime), and a regime with stronger contrast where the front re-forms after being deformed ("crack bridging"). In all the works mentioned above, both phases have the same elastic moduli and the crack is constrained to advance in its initial plane.

Gao [23] used a first-order perturbation analysis (in the spatial variations of elastic moduli) to show that spatially varying elastic moduli have an influence on the stress intensity factor at the tip of a crack. Although he did not pursue the derivation of an effective toughness in such a heterogeneous medium, a straightforward consequence of his analysis is that such an effective toughness should also depend on the elastic contrast between the phases.

So far, all these analysis assumed that the crack remained coplanar. However when inclusions are three-dimensional (for instance spheres), out-of-plane excursions of the crack are very likely and neglecting the out-of-plane bypassing mechanism of the inclusions may lead to an over-estimation of the effective fracture energy (sometimes equal to, or greater than, the average of the fracture energies of the phases, the so-called rule of mixtures). In a recent work Lebihain *et al* [30, 31], exploiting numerically the perturbation analysis of Gao and Rice and taking into account the possible bypassing of inclusions in addition to their in-plane crossing, report predictions of the effective toughness below the rule of mixtures. They also observe a zig-zag variation with time of the energy restitution rate and ask themselves the question of which value of the ERR should be taken, maximum value or average value? We will also come back to this point in the discussion.

Taking advantage of the computational capabilities offered by the variational model of Francfort and Marigo [19]), Hossain *et al* [27], Hsueh *et al* [28], Brach *et al* [8] simulated numerically the propagation of a crack in a heterogeneous medium, examining both the effect of a contrast in elasticity and in the fracture energy of the phases. They did observe

an effect of the elastic contrast of the phases, just as Gao did. They also observed a zig-zag variation of the ERR during crack propagation and choose the maximum value of this ERR in their definition of the effective fracture energy.

All the works mentioned so far are interested in the propagation of a *pre-existing* crack and in the interaction of the crack front with the obstacles formed by the inclusions. In addition, in most of the numerical studies following the crack advance and therefore monitoring the variations of the ERR with time, the definition of the effective fracture energy is based on the maximum value of the ERR.

By contrast, Schneider [45] has recently proposed a variational definition of the fracture energy that does not assume the existence of a pre-existing crack, is valid for any microstructure and is not based on the estimation of a local ERR field at a crack tip (or front). His definition is based on rigorous and explicit mathematical results which makes its computation doable. It is the objective of the present study to assess this definition and its relevance to a physically motivated definition of the effective fracture energy of a heterogeneous material discussed in section 6 and which can be formulated as

Definition ($\mathcal{D}$)**:** *The effective fracture energy in the direction* $\boldsymbol{\nu}$ *is the dissipated energy along the actual path of a crack in the unit cell with a normal vector equal in average to* $\boldsymbol{\nu}$ *leading to full fracture of the unit cell.*

Let us begin with a brief reminder of Schneider's approach to this problem. Following the variational model of Bourdin *et al* [6] generalizing Griffith's analysis, the propagation of a crack in an elastic, brittle solid can be viewed as the minimization at time t of the following global energy over $\boldsymbol{u}$ (the displacement field) and Γ (the crack location),

$$\int_{\Omega-\Gamma} \frac{1}{2}\boldsymbol{e}(\boldsymbol{u}) : \boldsymbol{C}^{\varepsilon}(\boldsymbol{X}) : \boldsymbol{e}(\boldsymbol{u})\, d\boldsymbol{X} \;+\; \int_{\Gamma} \gamma^{\varepsilon}(\boldsymbol{X}) d\mathcal{H}^{d-1}, \tag{1}$$

where d is the dimension of space, $\boldsymbol{u}$ satisfies some boundary condition $\boldsymbol{u} = \boldsymbol{U}(t)$ on $\partial\Omega$, $\boldsymbol{e}(\boldsymbol{u})$ is the symmetric part of the displacement gradient[2] $\boldsymbol{\nabla}_{\boldsymbol{X}}\boldsymbol{u}$, ε is a small parameter, typically the size of the inclusions which will eventually tend to 0, $\boldsymbol{C}^{\varepsilon}(\boldsymbol{X})$ is a fourth-order stiffness tensor, with minor and major symmetries taking different values in the different phases and strictly bounded from above and below, $\gamma^{\varepsilon}(\boldsymbol{X})$ is the *fracture energy of the material* again taking different values in the different phases. The actual crack location Γ^{ε} (minimizer of (1) with respect to Γ) satisfies a growth condition entailing the fact that

[2]Throughout the paper $\boldsymbol{X}$ denotes the macroscopic variable, whereas $\boldsymbol{x}$ stands for the microscopic space variable. When necessary, the differential operators (gradient, divergence) with respect to one variable or the other are denoted with a subscript $_{\boldsymbol{X}}$ or $_{\boldsymbol{x}}$. The subscript is omitted when the context is clear.

the crack propagation is dissipative and irreversible. Bourdin *et al* [6] emphasize that there are two different variational approaches to fracture depending on whether one looks for *local* or for *global* minimizers of (1).

Assuming, with Schneider, that the problem of interest is the *global* minimization of (1), then after time discretization we are led to the following variational problem at time t_{n+1},

$$\inf_{\boldsymbol{u}|_{\partial\Omega} = \boldsymbol{U}(t_{n+1})} \inf_{\Gamma_u \supseteq \Gamma_n^\varepsilon} \int_{\Omega - \Gamma_u} \frac{1}{2} \boldsymbol{e}(\boldsymbol{u}) : \boldsymbol{C}^\varepsilon(\boldsymbol{X}) : \boldsymbol{e}(\boldsymbol{u}) \, d\boldsymbol{X} \; + \; \int_{\Gamma_u} \gamma^\varepsilon(\boldsymbol{X}) d\mathcal{H}^{d-1}, \tag{2}$$

where Γ_n^ε is the location of the crack at time t_n, $\boldsymbol{u}$ and $\Gamma = \Gamma_u$ are the displacement field and crack location at time t_{n+1}.

Rigorous homogenization results for energies in the form (2) consisting of a bulk energy and a surface energy, *but without the irreversibility condition* $\Gamma \supseteq \Gamma_n^\varepsilon$, are available in the mathematical literature and are briefly recalled in section 2. One of the most remarkable result of these rigorous analyses (Braides *et al* [10], Crismale *et al* [14]) is that, under rather mild assumptions satisfied here, the bulk energy and the surface energy can be homogenized separately. The homogenized (or effective) bulk energy is given by the classical "average variational principle" (minimum of the energy over all fields under a prescribed average gradient and periodic deviation from its average) and does not depend on the surface energy. The construction of the homogenized (or effective) surface energy is more complicated, but it should be emphasized that it does not depend on the bulk (elastic) energy of the phases. First, all possible multiples of the unit cell are to be considered. Then, these multiple unit cells are rotated and a surface cutting these multiple of the unit cell is searched for, which is minimum for a "weighted" metric, the weight being the local distribution of the surface energy $\gamma(\boldsymbol{x})$ in the unit cell, with the average normal vector to this surface being prescribed. This minimization problem is nonconvex (at least at first sight). But an equivalent characterization of the homogenized surface energy has been provided (Braides and Chiàdo Piat [9], Chambolle and Thouroude [12]) in the form of the minimization of the total variation of a scalar function defined on a single unit cell, again weighted by the local surface energy, with a prescribed average gradient. It is therefore a much simpler convex problem. This problem is quite similar to a limit load problem (or yield design problem according to the terminology of Salençon [44]). By duality the determination of the effective surface energy (the effective plastic dissipation in the limit load analogy) is equivalent to the determination of a convex set in $\mathbb{R}^d$, quite similar to the effective flow surface in homogenization of composite materials with limited strength and standard methods can therefore be applied ([34, 50, 38] among others). Our algorithm of choice for the determination of this convex set is an incremental

plasticity algorithm which is applied in section 5 to compute minimum cuts for different microstructures.

With this equivalent formulation, the problem becomes much simpler and bounding techniques developed in the past 30 years in nonlinear homogenization (Ponte Castañeda and Suquet [42] for a partial review) can be applied in section 4 to obtain upper bounds to this effective surface energy. Finally section 6 addresses the question of whether the effective surface energy determined through variational principles is the "effective fracture energy" of the material as suggested by Schneider [45]. A proper, mathematically sound, definition of the effective fracture energy is still lacking and several definitions have been proposed (as noticed for instance by Lebihain *et al* [31]). When definition ($\mathcal{D}$) is adopted, the effective surface energy discussed here is a rigorous lower bound to the effective fracture energy of the composite and may be different from it in certain circumstances.

2 Mathematical preliminaries: bulk energy, surface energy and homogenization

In his definition of the effective toughness of a heterogeneous brittle material, Schneider [45] considers the variational problem

$$\inf_{\boldsymbol{u}|_{\partial\Omega}=\boldsymbol{U}} \int_{\Omega-\Gamma_u} \frac{1}{2}\boldsymbol{e}(\boldsymbol{u}) : \boldsymbol{C}^\varepsilon(\boldsymbol{X}) : \boldsymbol{e}(\boldsymbol{u})\, d\boldsymbol{X} \;+\; \int_{\Gamma_u} \gamma^\varepsilon(\boldsymbol{X}) d\mathcal{H}^{d-1}, \tag{3}$$

which is a simplified version of (2) *where the irreversibility condition* $\Gamma \supseteq \Gamma_n^\varepsilon$ *has been left aside*. The functional (3) falls in the more general class of functionals of the type

$$\int_\Omega f^\varepsilon(\boldsymbol{\nabla u})\, d\boldsymbol{X} \;+\; \int_{S_u} g^\varepsilon\left((\boldsymbol{u}^+ - \boldsymbol{u}^-)\otimes \boldsymbol{n_u}\right) d\mathcal{H}^{d-1}, \tag{4}$$

where Ω is a domain in $\mathbb{R}^d$, $\boldsymbol{u}$ is a vector field with values in $\mathbb{R}^m$ (m can be arbitrary, but we shall consider only $m = d$ which is the case of interest here), possibly with discontinuities, more specifically a special function with bounded variation, whose gradient $\boldsymbol{Du}$ in the sense of distributions can be split into two components, the first component $\boldsymbol{\nabla_X u}$ being regular (absolutely continuous with respect to the Lebesgue measure $\mathcal{L}^d$ on Ω) with density $\boldsymbol{\nabla u}$, and the second component being a measure concentrated on S_u

$$\boldsymbol{Du} = \boldsymbol{\nabla_X u}\; \mathcal{L}^d(\Omega) + (\boldsymbol{u}^+ - \boldsymbol{u}^-)\otimes \boldsymbol{n_u}\; \mathcal{H}^{d-1}(S_u), \tag{5}$$

where $\boldsymbol{n_u}$ is the normal vector to S_u.

In the case of interest here

$$f^\varepsilon(\boldsymbol{X}, \boldsymbol{\nabla u}) = \frac{1}{2}\boldsymbol{e}(\boldsymbol{u}) : \boldsymbol{C}^\varepsilon(\boldsymbol{X}) : \boldsymbol{e}(\boldsymbol{u}) = \frac{1}{2}\boldsymbol{\nabla u} : \boldsymbol{C}^\varepsilon(\boldsymbol{X}) : \boldsymbol{\nabla u}, \tag{6}$$

(the last equality (6) resulting from the symmetries of $\boldsymbol{C}$),

$$g^\varepsilon\left(\boldsymbol{X}, \boldsymbol{z} \otimes \boldsymbol{n}\right) = \begin{cases} 0 \text{ when } \boldsymbol{z} = \boldsymbol{0}, \\ \gamma^\varepsilon \text{ when } \boldsymbol{z} \neq \boldsymbol{0}. \end{cases} \tag{7}$$

Note that in the case of interest here, f^ε is convex, whereas g^ε is non-convex.

2.1 Surface energies and homogenization

Rigorous homogenization results exist in the literature for functionals of the type (4). The earliest result is due to Braides *et al* [10] which, unfortunately, holds under a growth assumption on f^ε with respect to $\boldsymbol{\nabla u}$ which is not satisfied here (since f^ε is a function of the symmetric part of $\boldsymbol{\nabla u}$ only). Friedrich *et al* [20] with the help of a result by Crismale *et al* [14] have partially[3] derived the Γ-limit of functionals in the form (4) under the following assumptions on f (assumed to be quasi-convex) and g

$$\left.\begin{array}{c} \alpha\left|\boldsymbol{\xi} + \boldsymbol{\xi}^{\mathsf{T}}\right|^p \leq f(\boldsymbol{X}, \boldsymbol{\xi}) \leq \beta(1 + \left|\boldsymbol{\xi} + \boldsymbol{\xi}^{\mathsf{T}}\right|^p),\ p > 1, \\ \alpha \leq g(\boldsymbol{X}, \boldsymbol{\xi}) \leq \beta, \end{array}\right\} \quad \text{a.e. } \boldsymbol{X} \in \mathbb{R}^d,\ \boldsymbol{\xi} \in \mathbb{M}^{d\times d}. \tag{8}$$

Friedrich *et al* [20] showed that the sequence (4) converges (in the sense of Γ-convergence) towards an energy in the same form

$$\int_\Omega f^{\text{hom}}(\boldsymbol{\nabla u})\, d\boldsymbol{X} \ + \ \int_{S_u} g^{\text{hom}}\left((\boldsymbol{u}^+ - \boldsymbol{u}^-) \otimes \boldsymbol{n}_{\boldsymbol{u}}\right) d\mathcal{H}^{d-1}. \tag{9}$$

For the sake of definiteness f^ε and g^ε are assumed to be periodic with respect to their first variable by translation along the unit cube $Q =]-\frac{1}{2}, \frac{1}{2}[^d$. Under this assumption explicit expressions of the homogenized limits f^{hom} and g^{hom} are available. The homogenized bulk energy f^{hom} is the "usual" homogenized bulk energy (homogenization with no surface energy) given by (Müller [40])

$$f^{\text{hom}}(\boldsymbol{\xi}) = \lim_{L\to+\infty} \inf_{\boldsymbol{u}^*} \frac{1}{|LQ|} \int_{LQ} f(\boldsymbol{x}, \boldsymbol{\nabla}_{\boldsymbol{x}}\boldsymbol{u}^* + \boldsymbol{\xi})\, d\boldsymbol{x}, \quad \boldsymbol{u}^* \in W_0^{1,p}(LQ, \mathbb{R}^d), \tag{10}$$

[3]Their result holds for general f^ε and g^ε satisfying (8) in dimension $d = 2$. When $d > 2$, it holds in full rigor when g^ε is independent of ε which in the present case means that all phases have the same fracture energy. We will assume that it also holds true in dimension $d = 3$ when g^ε depends on ε.

where[4] LQ is a multiple of the unit cube ($L = (L_1, ..., L_d)$, $LQ = \prod_{i=1}^{d} \left]-\frac{L_i}{2}, \frac{L_i}{2}\right[$) and $|LQ|$ denotes its measure (length, surface or volume depending on the space dimension d). When f is convex (which is the case here), the homogenized effective energy can be computed on a *single* unit cell with periodic trial fields $\boldsymbol{u}$ (Müller [40], Marcellini [33]),

$$f^{\text{hom}}(\boldsymbol{\xi}) = \inf_{\boldsymbol{u}^*} \frac{1}{|Q|} \int_Q f(\boldsymbol{x}, \boldsymbol{\nabla u}^* + \boldsymbol{\xi})\, d\boldsymbol{x}, \quad \boldsymbol{u}^* \in W^{1,p}_\sharp(Q, \mathbb{R}^d), \tag{11}$$

where the notation $\sharp$ denotes fields which are Q-periodic.

The expression for g^{hom} is as follows (recall that g is non-convex in the case of interest here) .

$$\left.\begin{array}{rcl} g^{\text{hom}}(\boldsymbol{z} \otimes \boldsymbol{\nu}) & = & \lim\limits_{L\to+\infty} \inf\limits_{\boldsymbol{u}} \dfrac{1}{|LQ|} \displaystyle\int_{LQ_{\boldsymbol{\nu}} \cap S_u} g\left(\boldsymbol{x}, (\boldsymbol{u}^+ - \boldsymbol{u}^-) \otimes \boldsymbol{n_u}\right)\, d\mathcal{H}^{d-1}, \\ & & \boldsymbol{u} \in SBV(LQ_{\boldsymbol{\nu}}, \mathbb{R}^d), \quad \boldsymbol{\nabla u} = \boldsymbol{0} \text{ a.e., } \boldsymbol{u} = \boldsymbol{u}_{\boldsymbol{z},\boldsymbol{\nu}} \text{ on } \partial(LQ_{\boldsymbol{\nu}}), \end{array}\right\} \tag{12}$$

where $LQ_{\boldsymbol{\nu}}$ is the multiple unit-cube with center in the origin and rotated in such a way that one of its faces is perpendicular to the unit vector $\boldsymbol{\nu}$, and

$$\boldsymbol{u}_{\boldsymbol{z},\boldsymbol{\nu}} = \left\{ \begin{array}{l} \boldsymbol{z} \text{ if } \boldsymbol{x}.\boldsymbol{\nu} \geq 0, \\ \boldsymbol{0} \text{ if } \boldsymbol{x}.\boldsymbol{\nu} < 0. \end{array}\right. \tag{13}$$

In the present problem g^{hom} can be simplified due to the specific form (7) of g. Since g does not depend on $\boldsymbol{z}$, the infimum in (12) does not depend either on $\boldsymbol{z}$ and consequently g^{hom} depends only on $\boldsymbol{\nu}$. It has the dimension of a surface energy and will denoted by $\gamma^{\text{hom}}(\boldsymbol{\nu})$. Similarly, since g does not depend on $\boldsymbol{n}_u$, but only on the existence of a discontinuity on S_u, attention can be limited to a scalar field u (with the same discontinuity set) instead of a vector field. Finally the variational problem defining the effective surface energy γ^{hom} reads as

$$\left.\begin{array}{rcl} \gamma^{\text{hom}}(\boldsymbol{\nu}) & = & \lim\limits_{L\to+\infty} \inf\limits_{u} \dfrac{1}{|LQ|} \displaystyle\int_{LQ_{\boldsymbol{\nu}} \cap S_u} \gamma(\boldsymbol{x})\, d\mathcal{H}^{d-1}, \\ & & u \in SBV(LQ_{\boldsymbol{\nu}}, \mathbb{R}), \quad \boldsymbol{\nabla} u = \boldsymbol{0} \text{ a.e. } LQ_{\boldsymbol{\nu}} - S_u, \\ & & u = 1 \text{ on } \partial(LQ_{\boldsymbol{\nu}}) \cap \{\boldsymbol{x}.\boldsymbol{\nu} \geq 0\},\ u = 0 \text{ on } \partial(LQ_{\boldsymbol{\nu}}) \cap \{\boldsymbol{x}.\boldsymbol{\nu} < 0\}. \end{array}\right\} \tag{14}$$

[4]It is again emphasized that in (10) $\boldsymbol{x}$ stands for the microscopic space variable. When necessary, the differential operators (gradient, divergence) with respect to one variable or the other are denoted with a subscript $\boldsymbol{X}$ or $\boldsymbol{x}$.

This variational problem for u is in fact a variational problem for the surface of discontinuity of u. Let E denote the subset of $LQ_{\boldsymbol{\nu}}$ where $u = 1$ and let S denote the part of ∂E (the boundary of E) which is not contained in $\partial LQ_{\boldsymbol{\nu}}$. Then a more comprehensive formulation of (14) is

$$\gamma^{\text{hom}}(\boldsymbol{\nu}) = \lim_{L\to+\infty} \inf_{S} \frac{1}{|LQ|} \int_{LQ_{\boldsymbol{\nu}}\cap S} \gamma(\boldsymbol{x})\, d\mathcal{H}^{d-1}, \tag{15}$$

where the infimum is taken over all surfaces S contained in $LQ_{\boldsymbol{\nu}}$ with a boundary included in $\partial(LQ_\nu)\cap\{\boldsymbol{x},\ \boldsymbol{x}.\boldsymbol{\nu} = 0\}$. In other words, (15) searches for the surface with the minimum $d-1$ area (weighted by γ) cutting the multiple-cell $LQ_{\boldsymbol{\nu}}$ in a direction orthogonal to $\boldsymbol{\nu}$. This problem is called the *minimum (or minimal) cut problem* (Strang [47, 48]).

In this form, it does not jump to the eyes that the infimum problem in (14) involves a convex function of u. Luckily an equivalent characterization of γ^{hom} has been given by Braides and Chiadò Piat ([9] and Chambolle and Thouroude [12]

$$\gamma^{\text{hom}}(\boldsymbol{\nu}) = \min_{u^*\in BV_\sharp(Q)} \frac{1}{|Q|} \int_{\overline{Q}} \gamma(\boldsymbol{x})|\boldsymbol{D}u^* + \boldsymbol{\nu}|, \tag{16}$$

where in the first equality the decomposition (5) of the measure $\boldsymbol{D}u^*$ holds and $BV_\sharp(Q)$ denotes the set of periodic BV functions[5] on $\mathbb{R}^d$.

It should be noted that the average of the energy is now taken on a single unit cell Q. Indeed, according to (15), (16) should again be posed on all multiples LQ of the unit cell and the limit as L tends to $+\infty$ should be taken. However, since the functional to be minimized is now a convex function of u (although not strictly convex), the convexity of this function allows to consider the average on a *single* unit cell (Müller [40]). γ^{hom} can alternatively be characterized using smooth functions (but in that case the energy minimum is not attained, hence the notation infimum instead of minimum)

$$\gamma^{\text{hom}}(\boldsymbol{\nu}) = \begin{array}{c}\text{Inf}\\ u = u^* + \boldsymbol{\nu}.\boldsymbol{x}\\ u^* \in W^{1,1}_\sharp(Q)\end{array} \quad \frac{1}{|Q|} \int_Q \gamma(\boldsymbol{x})|\boldsymbol{\nabla} u|\, d\boldsymbol{x}. \tag{17}$$

By construction, γ^{hom} is defined for $\boldsymbol{\nu}$ with norm 1. However the alternative characterization (17) can be used to extend the definition of γ^{hom} to any vector $\boldsymbol{\nu}$ and the resulting function γ^{hom} is positively homogeneous of degree 1. This allows for a dual characterization of γ^{hom} which will given in the next section.

[5] Alternatively Q can be thought of as a torus, the important point here being that since the measure $\boldsymbol{D}u^*$ might be positive on ∂Q, opposite sides of ∂Q should be counted only once.

Remark 1: Clearly, for a single unit cell Q, the right-hand side in (16) is less than the infimum in (15) (since characteristic functions of sets are admissible trial fields in (16)). In a slightly different setting Strang [47, 48] noticed that the minimizers in (16) are characteristic functions of sets with finite perimeter. Heuristically extrapolated to the present context, Strang's result gives a justification of the equality between the two infima. The equivalence (rigorously proved by Braides and Chiadò Piat [9] and Chambolle and Thouroude [12]) between (15) and (17) was intuited by Schneider [45] who used the formulation (17) in his numerical computations.

Remark 2: In view of the form (9) of the homogenized energy, $\gamma^{\rm hom}$ is called by Schneider [45] the *homogenized (or effective) crack resistance* of the material when $\gamma(\boldsymbol{x})$ is taken to be the material fracture energy at point $\boldsymbol{x}$. Section 6 will discuss this terminology, but for the time being $\gamma^{\rm hom}$ will be called the *effective surface energy* of the material.

Remark 3: It is surprising, at first, that no interaction takes place as ε tends to 0 between the bulk and the surface energies at the small scale. This is reflected in the fact that $f^{\rm hom}$ depends on f^ε *only* and that $g^{\rm hom}$ depends on g^ε *only*. In other words there is no influence of the elastic contrast on the effective surface energy and, conversely, no influence of the local surface energy on the bulk behaviour of the material.

Mathematically, this is a consequence of the bounding condition $(8)_2$ on g^ε. The situation is totally different when this condition is removed. For instance when g^ε has a linear growth with respect to $\boldsymbol{\xi}$, $f^{\rm hom}$ also has a linear growth with respect to $\boldsymbol{\xi}$ even for a quadratic f^ε (more details in Bouchitté *et al* [4]).

From a mechanical standpoint, an energetic argument provided by a referee during the review process of the present paper, may be used to explain why the local surface energy g does not enter the expression of the effective bulk energy $f^{\rm hom}$. Consider a two-dimensional body containing $1/\varepsilon^2$ cells of size ε. When the stiffness and the toughness of the components are independent of ε, the crack will cross only a few cells (at most $1/\varepsilon$), otherwise the contribution of the surface energy would be too large. Accordingly most of the cells remain unfractured and their behavior is, in the limit as ε goes to 0, governed by the usual effective elastic energy with no possibility of fracturing. The crack will only induce boundary layer effects in the neighborhood of the cracked cells for a cost of the order of ε in terms of the elastic energy.

However this argument does not show in turn why the effective surface energy $g^{\rm hom}$ should not depend on the local bulk energy f, or in other words why there is no influence of the elastic properties of the phases on the effective fracture energy of the composite, which is the most puzzling aspect of the decoupling between the two types of energy.

Remark 4: We will adopt in the remainder of this paper the variational characterization

(17) of the effective surface energy. However it should be noted that its initial definition (15) opens the way, at least in two-dimensional problems, to the use of purely geometrical algorithms developed in mathematical morphology to compute geodesics in random microstructures (see for instance Willot [56, 57]).

3 Limit loads, maximum flows and homogenization

3.1 Duality

As already pointed out, $\gamma^{\rm hom}$ defined by (17) is a (proper, lower-semi-continuous) convex function of $\boldsymbol{\nu}$ on $\mathbb{R}^d$ which is positively homogeneous of degree one. A classical result in convex analysis asserts that the Legendre-Fenchel transform of *any* such function (convex and positively homogeneous of degree one) is the indicator function (denoted $I_{P^{\rm hom}}$) of a convex set (denoted $P^{\rm hom}$) in $\mathbb{R}^d$

$$(\gamma^{\rm hom})^*(\boldsymbol{\Sigma}) = I_{P^{\rm hom}}(\boldsymbol{\Sigma}) = \left\{ \begin{array}{l} 0 \text{ if } \boldsymbol{\Sigma} \in P^{\rm hom}, \\ +\infty \text{ if } \boldsymbol{\Sigma} \notin P^{\rm hom}, \end{array} \right. \tag{18}$$

where $P^{\rm hom}$ is defined as

$$P^{\rm hom} = \{\boldsymbol{\Sigma} \text{ such that } \boldsymbol{\Sigma}.\boldsymbol{\nu} \leq \gamma^{hom}(\boldsymbol{\nu}) \text{ for all } \boldsymbol{\nu} \in \mathbb{R}^d\}. \tag{19}$$

An alternative characterization of $\gamma^{\rm hom}$ can be obtained by bi-duality,

$$\gamma^{\rm hom}(\boldsymbol{\nu}) = (\gamma^{\rm hom})^{**}(\boldsymbol{\nu}) = (I_{P^{\rm hom}})^*(\boldsymbol{\nu}) = \sup_{\boldsymbol{\Sigma} \in P^{\rm hom}} \boldsymbol{\Sigma}.\boldsymbol{\nu}\,. \tag{20}$$

In other words the *minimum cut* orthogonal in average to $\boldsymbol{\nu}$ (left-hand side of (20)) is equal to the *maximum flow* passing through Q in the direction of $\boldsymbol{\nu}$ (right-hand side of (20)) subject to the physical limitation $\boldsymbol{\Sigma} \in P^{\rm hom}$. It follows from (20) and (19) that one may either compute $\gamma^{\rm hom}$ or equivalently the convex set $P^{\rm hom}$ and get one quantity from the other.

In order to compute $P^{\rm hom}$ we need another characterization of this set through a problem posed on the unit cell. For this purpose, the characterization of the convex conjugate $(\gamma^{\rm hom})^*$ of $\gamma^{\rm hom}$ given in Bouchitté [3] (lemma 3.5, see also Bouchitté and Suquet [5]) may be used. By definition,

$$\gamma^{\rm hom}(\boldsymbol{\nu}) = \inf_{u = u^* + \boldsymbol{\nu}.\boldsymbol{x}} \frac{1}{|Q|} \int_Q \pi(\boldsymbol{x}, \boldsymbol{\nabla} u)\, d\boldsymbol{x}, \quad u^* \in W^{1,1}_\sharp(Q), \tag{21}$$

where

$$\pi(\boldsymbol{x}, \boldsymbol{z}) = \gamma(\boldsymbol{x}) \, |\boldsymbol{z}| \, . \tag{22}$$

Its convex dual can also be characterized by a variational property

$$(\gamma^{\text{hom}})^*(\boldsymbol{\Sigma}) = \inf_{\boldsymbol{\sigma} \, \in \, \mathcal{S}(\boldsymbol{\Sigma})} \frac{1}{|Q|} \int_Q \pi^*(\boldsymbol{x}, \boldsymbol{\sigma}) \, d\boldsymbol{x}, \tag{23}$$

where

$$\mathcal{S}(\boldsymbol{\Sigma}) = \left\{ \boldsymbol{\sigma} \in L^2(Q)^d, \ \text{div}_{\boldsymbol{x}} \boldsymbol{\sigma} = 0, \ \langle \boldsymbol{\sigma} \rangle = \boldsymbol{\Sigma}, \ \boldsymbol{\sigma}.\boldsymbol{n} - \sharp \right\}, \tag{24}$$

and the notation $-\sharp$ denotes fields taking opposite values on opposite sides of Q. In addition, making reasonable assumptions on the dependence of $\gamma(\boldsymbol{x})$ on $\boldsymbol{x}$, the dual π^* of π is the indicator function of the ball of radius $\gamma(\boldsymbol{x})$ and reads as

$$\pi^*(\boldsymbol{x}, \boldsymbol{\tau}) = \begin{cases} 0 \text{ if } \ |\boldsymbol{\tau}| \leq \gamma(\boldsymbol{x}), \\ +\infty \text{ otherwise.} \end{cases} \tag{25}$$

These smoothness assumptions are in particular fulfilled when,

(H1) Q is partitioned into N open sets $Q^{(r)}$ (the different phases) which are such that $Q^{(r)} \cap Q^{(s)} = \emptyset$ when $r \neq s$ and $\overline{Q} = \bigcup_{r=1}^{N} \overline{Q}^{(r)}$,

(H2) $\gamma(\boldsymbol{x}) = \gamma^{(r)}$ is uniform (strictly positive and finite) in each subdomain $Q^{(r)}$. In particular there exist constants γ_1 and γ_2 such that

$$0 < \gamma_1 \leq \gamma(\boldsymbol{x}) \leq \gamma_2 < +\infty \quad a.e. \quad Q. \tag{26}$$

It follows from (25) that $(\gamma^{\text{hom}})^*$ is the indicator function of the convex set

$$\begin{aligned} P^{hom} \ &= \{ \boldsymbol{\Sigma} \in \mathbb{R}^d \text{ such that } \exists \, \boldsymbol{\sigma}(\boldsymbol{x}), \text{ satisfying} \\ &\langle \boldsymbol{\sigma} \rangle = \boldsymbol{\Sigma}, \ \text{div}_{\boldsymbol{x}} \boldsymbol{\sigma} = \boldsymbol{0}, \ \boldsymbol{\sigma}.\boldsymbol{n} - \sharp, \text{ and } \ |\boldsymbol{\sigma}(\boldsymbol{x})| \leq \gamma(\boldsymbol{x}) \text{ a.e. } Q \}. \end{aligned} \tag{27}$$

3.2 Limit loads: static, kinematic and saddle-point formulations

The characterization (27) of the effective flow surface P^{hom} is the strict analogue (in a vectorial setting, also sometimes referred to as the conductivity setting) of the overall flow surface of composite materials with a limited strength, a problem which arises when dealing with the homogenization of limit loads in a tensorial setting (tensors of order 2).

For the sake of clarity, we give here a brief reminder on limit load problems. Consider a macroscopic solid body Ω subjected to body forces $\lambda \boldsymbol{f}$ and surface tractions $\lambda \boldsymbol{F}$ on a part $\partial\Omega_F$ of its boundary, proportional to a loading parameter λ. Neglecting the geometry changes of the body, the equilibrium equations between the loading and the stress field read as

$$\mathrm{div}_{\boldsymbol{X}} \boldsymbol{\sigma} + \lambda \boldsymbol{f} = \boldsymbol{0} \quad \text{in } \Omega, \quad \boldsymbol{\sigma}.\boldsymbol{n} = \lambda \boldsymbol{F} \text{ on } \partial\Omega_F, \tag{28}$$

where $\boldsymbol{\sigma}$ is now a second-order symmetric tensor field. The body is comprised of a material, possibly heterogeneous with a limited strength characterized by a *strength* domain $P(\boldsymbol{X})$ (convex set containing $\boldsymbol{0}$ in its interior)

$$\boldsymbol{\sigma}(\boldsymbol{X}) \ \in \ P(\boldsymbol{X}) \quad \text{in } \Omega. \tag{29}$$

The limit load problem is

$$\overline{\lambda} = \ \textbf{Maximize } \lambda \textbf{ subject to (28) and (29)}. \tag{30}$$

This *static* definition of the limit load (in term of stress fields) admits an equivalent mixed formulation (saddle-point)

$$\overline{\lambda} = \inf_{\boldsymbol{v}} \ \sup_{\boldsymbol{\tau} \in P} \frac{\int_\Omega \boldsymbol{\tau} : \boldsymbol{e}(\boldsymbol{v}) \, d\boldsymbol{X}}{\int_\Omega \boldsymbol{f}.\boldsymbol{v} \, d\boldsymbol{X} + \int_{\partial\Omega_F} \boldsymbol{F}.\boldsymbol{v} \, ds}, \tag{31}$$

and an equivalent kinematic formulation (minimum principle)

$$\overline{\lambda} = \inf_{\boldsymbol{v}, \ L(\boldsymbol{v}) = 1} \int_\Omega \pi(\boldsymbol{X}, \boldsymbol{e}(\boldsymbol{v})) \, d\boldsymbol{X}, \tag{32}$$

where

$$\pi(\boldsymbol{X}, \boldsymbol{e}) = \sup_{\boldsymbol{\tau} \in P(\boldsymbol{X})} \boldsymbol{\tau} : \boldsymbol{e}, \text{ and } L(\boldsymbol{v}) = \int_\Omega \boldsymbol{f}.\boldsymbol{v} \, d\boldsymbol{X} + \int_{\partial\Omega_F} \boldsymbol{F}.\boldsymbol{v} \, ds. \tag{33}$$

π is called the (plastic) dissipation associated with the (plastic) failure mode $\boldsymbol{v}$.

So far, the only assumption on the constitutive law of the constituents, is the constraint that the stress tensor $\boldsymbol{\sigma}(\boldsymbol{x})$ must stay in the domain $P(\boldsymbol{x})$ of physically admissible stress states. There is no further assumption, such as a normality rule, made on the constitutive relations of the phases. However, mathematically the Euler-Lagrange equations associated with the minimization problem (32) are formally identical to that of a rigid-plastic material. This analogy is easily seen by writing the minimization problem (32) as follows. Assuming for simplicity that $\partial\Omega_F = \emptyset$, $\boldsymbol{v} = 0$ on $\partial\Omega$ and that $P(\boldsymbol{X})$ is

characterized by the inequality $f(\boldsymbol{X},\boldsymbol{\sigma}) \leq 0$, the saddle point problem (31) is re-written as

$$\left.\begin{aligned} \overline{\lambda} &= - \inf_{\boldsymbol{v},\ L(\boldsymbol{v})=1} \ \inf_{\boldsymbol{\tau} \in P} \int_\Omega -\boldsymbol{\tau} : \boldsymbol{e}(\boldsymbol{v})\, d\boldsymbol{X} \\ &= - \inf_{\boldsymbol{v}} \inf_{\boldsymbol{\tau}} \sup_{\Lambda} \sup_{\theta \geq 0} \int_\Omega -\boldsymbol{\tau} : \boldsymbol{e}(\boldsymbol{v})\, d\boldsymbol{X} + \Lambda(L(\boldsymbol{v})-1) + \int_\Omega \theta(\boldsymbol{X}) f(\boldsymbol{X},\boldsymbol{\tau})\, d\boldsymbol{X}. \end{aligned}\right\} \tag{34}$$

where Λ is the (scalar) Lagrange multiplier associated with the constraint $L(\boldsymbol{v}) = 1$ and θ is a (field of) Lagrange multiplier associated with the pointwise constraint $f(\boldsymbol{X},\boldsymbol{\tau}) \leq 0$. The optimality conditions for (34) with respect to $\boldsymbol{v}, \theta, \boldsymbol{\tau}, \Lambda$ (in this order) read as, denoting as $\dot{\boldsymbol{u}}, \dot{p}, \boldsymbol{\sigma}, \lambda$ the optimal solution,

$$\left.\begin{aligned} &\mathrm{div}_{\boldsymbol{X}} \boldsymbol{\sigma} + \lambda \boldsymbol{f} = \boldsymbol{0}, \quad f(\boldsymbol{X},\boldsymbol{\sigma}(\boldsymbol{X})) \leq 0 \text{ a.e. in } \Omega, \quad \dot{\boldsymbol{u}} = 0 \text{ on } \partial\Omega, \\ &\boldsymbol{e}(\dot{\boldsymbol{u}}(\boldsymbol{X})) = \dot{p}(\boldsymbol{X}) \frac{\partial f}{\partial \boldsymbol{\sigma}}(\boldsymbol{X},\boldsymbol{\sigma}), \quad L(\dot{\boldsymbol{u}}) = 1. \end{aligned}\right\} \tag{35}$$

According to these relations, $\dot{\boldsymbol{u}}$ is a nonvanishing velocity field (because of the last equation in (35)), $\boldsymbol{\sigma}$ is in equilibrium with $\lambda \boldsymbol{f}$, $\boldsymbol{\sigma}$ satisfies the constraint $f(\boldsymbol{\sigma}) \leq 0$ in Ω, $\boldsymbol{\sigma}$ and $\boldsymbol{e}(\dot{\boldsymbol{u}})$ are related by the normality rule (first equation in the second line of (35). In other words, the optimality conditions are nothing else than the equations for the equilibrium of a rigid-plastic body with normality rule (and λ is the limit load)

Limit-load analysis is a classical chapter in the engineering literature where it is often associated with plasticity (see [16] for instance) for the reason that we have just seen. However there is no limitation to plastic bodies in the above formulation which therefore applies to a wide variety of materials with limited strength, ranging from brittle materials to ideally plastic ones. This observation motivated several authors to call "yield design" the study of limit loads and limit states without reference to plasticity (Salençon [44]).

The equivalence between the three formulations, static (30), kinematic (32) and saddle-point (31) has long being recognized at least formally. Mathematically it is valid under technical assumptions on $P(\boldsymbol{X})$ generalizing (26) which are satisfied by usual criteria (including the von Mises criterion) and which consist essentially in assuming that all domains $P(\boldsymbol{X})$ are bounded from below and from above (*i.e.*, they contain a fixed ball of nonzero radius and are contained in a fixed ball of finite radius) either in stress space or in the space of deviators. These three formulations have been extensively used in many different computational methods (see section 5.1 for a nonexhaustive list of references).

Limit-load analysis has been extended along the years in several directions and one of these extensions, especially relevant here, deals with multiple loading parameters, when

the loading depends not only on a single parameter but on a m-dimensional array of parameters $\boldsymbol{\lambda}$. The theory, not developed here, leads to the definition of a convex safety domain in the space $\mathbb{R}^m$ of loading parameters instead of a single interval for one-parameter loadings.

Homogenization of limit loads has been considered in Bouchitté [3] (when there is no load on the boundary) and Bouchitté and Suquet [5] (for the case of loaded boundaries). Consider a highly heterogeneous body, characterized by a small parameter ε measuring the size of the heterogeneities and a highly oscillating domain $P^\varepsilon(\boldsymbol{x})$ in which the stress field is constrained to stay. For simplicity only the periodic case is considered here. The limit as $\varepsilon \to 0$ of the limit load problem is again solution of a limit load problem :

$$\overline{\lambda} = \lim_{\varepsilon \to 0} \overline{\lambda}^\varepsilon = \mathrm{Sup}\{\lambda \text{ such that } \exists\, \boldsymbol{\Sigma}(\boldsymbol{X}) \text{ satisfying (28) and (38)}\}, \tag{36}$$

where the material constraints homogenizing (29) are now

$$\boldsymbol{\Sigma} \in \ P^{hom} \text{ in } \Omega,\ \boldsymbol{\Sigma}.\boldsymbol{n} \ \in \ C^{hom} \text{ on } \partial\Omega_F, \tag{37}$$

with[6]

$$\begin{aligned} P^{\mathrm{hom}} \ &= \{\boldsymbol{\Sigma} \in \mathbb{R}^{d\times d}_s \text{ such that } \exists\, \boldsymbol{\sigma}(\boldsymbol{x}),\ \text{satisfying} \\ &\quad \langle \boldsymbol{\sigma} \rangle = \boldsymbol{\Sigma},\ \mathrm{div}_{\boldsymbol{x}} \boldsymbol{\sigma} = \boldsymbol{0},\ \boldsymbol{\sigma}.\boldsymbol{n} \ -\sharp,\ \boldsymbol{\sigma}(\boldsymbol{x}) \in P(\boldsymbol{x}) \text{ a.e. in } Q\}, \end{aligned} \tag{38}$$

where $\langle . \rangle$ stands for the volume average over a unit cell Q.

Concentrating on the bulk behavior, the homogenized strength domain is determined by solving the (generalized) limit load problem (38) on a unit cell Q, with $d(d+1)/2$ loading parameters (instead of a single one) which are the $d(d+1)/2$ independent components of the symmetric second-order tensor $\boldsymbol{\Sigma}$ whose components play the role of the multiple loading parameters mentioned above.

A dual characterization of P^{hom} may be obtained,

$$P^{\mathrm{hom}} = \{\boldsymbol{\Sigma} \text{ such that } \boldsymbol{\Sigma} : \boldsymbol{E} \leq \pi^{hom}(\boldsymbol{E}) \text{ for all } \boldsymbol{E} \in \mathbb{R}^{d\times d}_s\}, \tag{39}$$

where

$$\pi^{hom}(\boldsymbol{E}) = \inf_{\boldsymbol{u}} \quad \langle \pi(\boldsymbol{e}(\boldsymbol{u})) \rangle, \quad \boldsymbol{u} = \boldsymbol{E}.\boldsymbol{x} + \boldsymbol{u}^*,\ \boldsymbol{u}^* \in W^{1,1}_\sharp(Q)^d. \tag{40}$$

[6]The homogenized stress domain C^{hom} on the boundary is not directly deduced from the strength domain P^{hom} in the bulk of the body, indicating a discrepancy between the behavior in bulk and on the boundary which is uncommon in homogenization. This point is not important for the problem under consideration here.

Since π^{hom} and $\boldsymbol{\Sigma} : \boldsymbol{E}$ are both positively homogeneous of degree 1, it is sufficient to consider $\boldsymbol{E}$ with norm 1 in (39).

In conclusion the problem of finding the admissible domain of maximum flows is quite similar to that of limit loads, and even simpler since the "flow" or "stress" $\boldsymbol{\Sigma}$ is a vector in the maximum flow problem, instead of being a symmetric second-order tensor in the limit load problem. Therefore *the effective surface energy γ^{hom} can be obtained as the maximal dissipation of a specific limit load problem with d independent components (the components of $\boldsymbol{\Sigma}$), with d associated kinematic variables (the components of $\boldsymbol{\nu}$). And the determination of the surface energy can be alternatively done through the determination of the convex domain P^{hom}.* This analogy between limit loads and effective surface energy will be exploited in the next two sections.

4 Bounds

Upper bounds or estimates for the effective energy (17) may be derived in (almost) closed form by means of different variational techniques developed in the past two decades for nonlinear composites. As already noticed, the problem at hand is very similar to that of extremal flow surfaces addressed for instance in Suquet [51]. A first set of elementary bounds consists of the Voigt upper bound (or rule of mixtures), obtained by choosing $u^* = 0$ in (17), and the Reuss bound, obtained by choosing $\boldsymbol{\sigma} = \boldsymbol{\Sigma}$ in (27),

$$\inf_{\boldsymbol{x} \in \Omega} \gamma(\boldsymbol{x}) \leq \gamma^{\text{hom}} \leq \langle \gamma \rangle. \tag{41}$$

More accurate upper bounds can be obtained by techniques based on a linear comparison composite which have proven to be quite fruitful for plastic or viscoplastic phases [41, 51, 42]. Although the variational technique of Ponte Castañeda [41] is more general, we give in section 4.1 a direct derivation of these variational bounds following Suquet [51, 52]. For simplicity, attention is restricted in section 4.2 to isotropic materials and to isotropic linear comparison composites.

4.1 Variational upper bound *à la* Cauchy-Schwarz

Thanks to the Cauchy-Schwarz inequality we note that, for any nonnegative field $\mu(\boldsymbol{x})$

$$\langle \gamma \, |\boldsymbol{\nabla} u| \rangle \leq \left\langle \frac{\gamma^2}{\mu} \right\rangle^{1/2} \langle \mu \, |\boldsymbol{\nabla} u|^2 \rangle^{1/2}, \tag{42}$$

and that by choosing $\mu(\boldsymbol{x}) = \gamma(\boldsymbol{x})/\left|\boldsymbol{\nabla} u(\boldsymbol{x})\right|$, one has

$$\langle \gamma \left|\boldsymbol{\nabla} u\right| \rangle = \inf_{\mu(\boldsymbol{x}) \geq 0} \left\langle \frac{\gamma^2}{\mu} \right\rangle^{1/2} \langle \mu \left|\boldsymbol{\nabla} u\right|^2 \rangle^{1/2}. \tag{43}$$

Upon minimizing both sides of (43) over u, one gets another variational characterization of the infimum in (17)

$$\gamma^{\mathrm{hom}}(\boldsymbol{\nu}) = \inf_{\mu(\boldsymbol{x}) \geq 0} \left\langle \frac{\gamma^2}{\mu} \right\rangle^{1/2} w^{\mathrm{hom}}(\mu, \boldsymbol{\nu})^{1/2}, \tag{44}$$

where $w^{\mathrm{hom}}(\mu, .)$ is the effective (quadratic) energy of a linear composite with modulus (or conductivity) $\mu(\boldsymbol{x})$ at point $\boldsymbol{x}$. Finally taking the field $\mu(\boldsymbol{x})$ uniform in each phase ($\mu^{(r)}$ in phase r) the following upper bound is obtained

$$\gamma^{\mathrm{hom}}(\boldsymbol{\nu}) \leq \inf_{\mu^{(r)} \geq 0} \left\langle \frac{\gamma^2}{\mu} \right\rangle^{1/2} w^{\mathrm{hom}}(\mu^{(r)}, \boldsymbol{\nu})^{1/2}. \tag{45}$$

4.2 Isotropic composites.

When the composite under consideration is a N-phase isotropic composite, the effective surface energy does not depend on the direction of $\boldsymbol{\nu}$ and is characterized by a single scalar

$$\gamma^{\mathrm{hom}}(\boldsymbol{\nu}) = \gamma^{\mathrm{hom}} \left|\boldsymbol{\nu}\right|.$$

Similarly the effective energy w^{hom} of the linear comparison is characterized by a single effective modulus μ^{hom} and evaluating the bound (45) amounts to optimizing the function $\mu^{(r)}|_{r=1,..,N} \rightarrow \left\langle \frac{\gamma^2}{\mu} \right\rangle \mu^{\mathrm{hom}}$ with respect to the (positive) phase moduli $\mu^{(r)}$. The corresponding optimality conditions read as

$$c^{(r)} \left(\frac{\gamma^{(r)}}{\mu^{(r)}} \right)^2 = \frac{\partial \mu^{\mathrm{hom}}}{\partial \mu^{(r)}}, \quad r = 1, ..., N. \tag{46}$$

For definiteness let us consider a two-phase isotropic composite with a microstructure such that its effective linear properties are well described by one of the Hashin-Shtrikman bounds

$$\mu^{\mathrm{hom}} = \mu^{(2)} + c^{(1)}(\mu^{(1)} - \mu^{(2)}) \frac{d\mu^{(2)}}{d\mu^{(2)} + c^{(2)}(\mu^{(1)} - \mu^{(2)})}, \tag{47}$$

where d is the dimension of space. A straightforward calculation shows that the moduli in the linear composite which solve (46), are solutions of the nonlinear equation

$$\frac{\mu^{(1)}}{\mu^{(2)}} = \frac{\gamma^{(1)}}{\gamma^{(2)}} \left[1 + \frac{c^{(2)} + dc^{(1)}}{d^2} \left(\frac{\mu^{(1)}}{\mu^{(2}} - 1\right)^2 + \frac{2}{d} \left(\frac{\mu^{(1)}}{\mu^{(2}} - 1\right)\right]^{1/2}. \tag{48}$$

The solution of this nonlinear equation reads as follows.

a) When $\dfrac{\gamma^{(1)}}{\gamma^{(2)}} \leq \dfrac{d}{\sqrt{c^{(2)} + dc^{(1)}}}$, the solution of (48) is

$$\frac{\mu^{(1)}}{\mu^{(2)}} = \frac{c^{(2)}(d-1) + d\sqrt{(d-1)\left(\dfrac{d - c^{(2)}}{r^2}\right) - c^{(1)}}}{\dfrac{d^2}{r^2} - (c^{(2)} + dc^{(1)})}, \quad \text{where } r = \frac{\gamma^{(1)}}{\gamma^{(2)}}, \tag{49}$$

and the corresponding upper bound (45) is

$$\frac{\gamma^{\text{hom}}}{\gamma^{(2)}} \leq \left(\frac{\mu^{\text{hom}}}{\mu^{(2)}}\right)^{1/2} \left(c^{(1)} \frac{\mu^{(2)}}{\mu^{(1)}} r^2 + c^{(2)}\right)^{1/2}, \tag{50}$$

where $\dfrac{\mu^{\text{hom}}}{\mu^{(2)}}$ and $\dfrac{\mu^{(1)}}{\mu^{(2)}}$ are given by (47) and (49) respectively.

b) When $\dfrac{\gamma^{(1)}}{\gamma^{(2)}} \geq \dfrac{d}{\sqrt{c^{(2)} + dc^{(1)}}}$ the nonlinear equation (48) has no positive solution. The minimum with respect to $\mu^{(1)}/\mu^{(2)}$ of the function under consideration is attained on the boundary of the interval $[0, +\infty)$. The result is

$$\frac{\mu^{(1)}}{\mu^{(2)}} = +\infty, \quad \frac{\gamma^{\text{hom}}}{\gamma^{(2)}} = \sqrt{c^{(2)} + dc^{(1)}}. \tag{51}$$

In other words, when arranging the two phases in such a way that the effective *linear* conductivity of the composite is given by the relation (47), the maximum effective surface energy that one can get, irrespective of how large is the energy of phase 1, is $\gamma^{(2)}\sqrt{c^{(2)} + dc^{(1)}}$. This maximum value is reached when the contrast between the effective energy of the phases is larger than the critical ratio $\dfrac{d}{\sqrt{c^{(2)} + dc^{(1)}}}$. Increasing the ratio of

surface energies above this ratio does not yield any further overall strengthening of the material.

Remark 5. Anticipating on section 5, we note that the threshold captured by the upper bound (51) is consistent with the numerical simulations and with physical intuition. If one thinks of a matrix reinforced by spherical particles, it is likely that below a certain contrast in toughness between the phases it will be energetically more favorable for the crack to cross the particles, whereas above a certain contrast it will be energetically less costly to bypass them. In the bypassing regime the toughness of the inclusion can be increased at will without any change in the crack configuration (and in the effective energy). Hence the threshold effect which corresponds to a switch in the cracking mechanism from crossing to bypassing of inclusions.

Remark 6. Although the upper bound (45) sounds rather elementary, no better bound is available to the authors'knowledge (although better *estimates* can certainly be derived but without a rigorous bounding character). However, as already indicated in remark 4, section 2, the characterization of γ^{hom} in terms of minimum surfaces (or geodesics in dimension 2) can be used to derive bounds or estimates for specific microstructures. This has been done by Willot in dimension 2 when the microstructure consists of a Boolean arrangement of circular disks.

Remark 7. Similarly the Reuss bound is quite elementary. However it has been shown that it is optimal, even among isotropic microstructures. Indeed Garroni *et al* [24] showed that there exist isotropic microstructures for which the Reuss bound is exact for the problem of maximal flow (a similar conclusion was reached in dimension 2 by Suquet [53] by completely different means). Therefore, without any specific information about the microstructure besides its isotropy, the worst attainable case is the Reuss bound, i.e., the lowest energy among all constituents.

5 Sample examples

5.1 Computational procedure

Appropriate numerical schemes have been developed to solve the limit load problem using either the static formulation (30) or the kinematic formulation (32) or the saddle-point formulation (31). It has become a classical chapter in the computational engineering literature with classical continuous finite element approximations (Anderheggen and Knöpfel [1] among others), or less standard discontinuous displacement (or velocity) fields (Sloan and Kleeman [46] among others). It has also drawn attention in the applied mathematics literature (Matthies *et al* [35], Christiansen [13] among others). The associated compu-

tational schemes are either specifically designed for non-smooth functionals such as the function (32) which is not differentiable at the origin (like the total variation in image processing) or by using the saddle point formulation (Mercier ([37, 21], Schneider [45]), or by using more standard step-by-step schemes already available for elasto-plastic problems where the limit load is attained incrementally (or even in one "large" step in some analyses [32]).

The approach followed here belongs to the second category, where the limit load problem (30) is solved using an elasto-plastic scheme previously used in several other studies by the authors (for more details about the scheme, see section 2.3 of Suquet [49], section 3.2 of Michel *et al* [38] or Appendix A of Vincent *et al* [55]). The notations are chosen to highlight the similarities with limit loads computed as the limit of the solution of an elasto-plastic problem. u is a scalar field (scalar version of a displacement field), $\boldsymbol{e}(u) = \left(..., \frac{\partial u}{\partial x_i}, ...\right)$ is the gradient of u (analogue of the strain tensor field) and $\boldsymbol{\sigma} = (..., \sigma_i, ...)$ is a divergence-free vector field, analogue of the second-order stress field.

Artificial elastic properties are added to the actual strength properties of the material and the following evolution problem on the unit cell with appropriate periodicity conditions is solved along a path with imposed average strain rate,

$$\left.\begin{array}{c} \boldsymbol{e}(\dot{\boldsymbol{u}}) = \boldsymbol{\Lambda} : \dot{\boldsymbol{\sigma}} + \dot{\boldsymbol{e}}^{\mathsf{p}},\ \dot{\boldsymbol{e}}^{\mathsf{p}} = \dot{p}\dfrac{\partial f}{\partial \boldsymbol{\sigma}}(\boldsymbol{\sigma}),\ \dot{p} \geq 0,\ f(\boldsymbol{\sigma}) \leq 0,\ \dot{p} f(\boldsymbol{\sigma}) = 0, \\ \mathrm{div}\boldsymbol{\sigma} = 0, \quad \dot{\boldsymbol{u}} = \boldsymbol{\nu}.\boldsymbol{x} + \dot{\boldsymbol{u}}^*, \\ \text{periodicity conditions on } \boldsymbol{u}^* \text{ and } \boldsymbol{\sigma}.\boldsymbol{n}. \end{array}\right\} \tag{52}$$

t is an artificial time and f is the yield criterion of the material which may vary from point to point. Here $f(\boldsymbol{x}, \boldsymbol{\sigma}) = |\boldsymbol{\sigma}|^2 - \gamma^2(\boldsymbol{x})$. The system of equations (52) is integrated in time until the average "stress" $\boldsymbol{\Sigma}(t) = \langle \boldsymbol{\sigma}(t) \rangle$ reaches a stationary value $\boldsymbol{\Sigma}^\infty$ which lies on the effective extremal surface with outer normal to the surface given by $\boldsymbol{\nu}$ (Suquet [50], Michel *et al* [38], section 3.2). As is classical in the computational homogenization of extremal surfaces for heterogeneous materials, this determination can be either performed following a strain-based approach (the strain-rate direction $\boldsymbol{\nu}$ is imposed- or a stress-based approach, the direction of $\boldsymbol{\Sigma}(t)$ is imposed). Both approaches deliver the same extremal surfaces. The stress based approach is more convenient when the extremal surface contains flat portions.

As is well-known in limit-load analysis, the asymptotic overall stress (or limit load) $\boldsymbol{\Sigma}^\infty$ does not depend on the added artificial elasticity, nor on the initial condition. By contrast, the local strain-rate field (in other words, the failure mode) may depend on the

choice of the artificial elasticity and/or the initial conditions, even though its average, by construction, is the same, $\boldsymbol{\nu}$.

In the problem under consideration here, the only small variation with respect to the above general scheme is that the stress field is a vector field instead of a symmetric tensor field. For simplicity, elasticity is assumed to be isotropic, characterized by a shear modulus μ (which will be uniform throughout the unit cell, unless otherwise specified). The time-discretized strain and stress fields $\boldsymbol{e}$ and $\boldsymbol{\sigma}$ at time t_{n+1} are obtained by iterating on the following system (all quantities at time t_n are labelled by a subscript n)

$$\text{Elastic prediction:} \left\{ \begin{array}{l} \boldsymbol{\sigma}^E = \Delta\boldsymbol{\sigma}^E + \boldsymbol{\sigma}_n, \quad \Delta\boldsymbol{\sigma}^E = \mu\Delta\boldsymbol{e}, \quad \Delta\boldsymbol{e} = (\boldsymbol{e}(u) - \boldsymbol{e}(u_n)), \\ u = t_{n+1}\boldsymbol{\nu}.\boldsymbol{x} + u^*, \quad u^* \text{ periodic on } \partial Q, \end{array} \right. \tag{53}$$

$$\text{Plastic correction:} \left\{ \begin{array}{l} \Delta\boldsymbol{\sigma} = \boldsymbol{\sigma} - \boldsymbol{\sigma}_n = \mu(\Delta\boldsymbol{e} - \Delta\boldsymbol{e}^{\mathsf{p}}), \quad \Delta\boldsymbol{e}^{\mathsf{p}} = \Delta p \dfrac{\partial f}{\partial \boldsymbol{\sigma}}(\boldsymbol{\sigma}), \\ \text{div}\boldsymbol{\sigma} = 0, \quad \boldsymbol{\sigma}.\boldsymbol{n} \text{ anti-periodic on } \partial Q. \end{array} \right. \tag{54}$$

The yield-like criterion is $f(\boldsymbol{\sigma}) = |\boldsymbol{\sigma}|^2 - \gamma^2 \leq 0$, and after eliminating $\boldsymbol{\sigma}_n$ between (53) and (54) the plastic correction can be expressed as

$$\Delta p = \frac{1}{2\mu}\left(\frac{\left|\boldsymbol{\sigma}^E\right|}{\gamma} - 1\right)^+, \; \boldsymbol{\sigma} = \left\{ \begin{array}{l} \boldsymbol{\sigma}^E \text{ when } \left|\boldsymbol{\sigma}^E\right| \leq \gamma, \\ \gamma\dfrac{\boldsymbol{\sigma}^E}{|\boldsymbol{\sigma}^E|} \text{ when } \left|\boldsymbol{\sigma}^E\right| > \gamma, \end{array} \right. \tag{55}$$

where $(.)^+$ denotes the positive part of a quantity.

In the plastic regime (i.e., when $\left|\boldsymbol{\sigma}^E\right| > \gamma$), the equality defining $\boldsymbol{\sigma}$ in the equation $(54)_1$ is a non-linear equation, so that the equilibrium condition $(54)_2$ to be met by $\boldsymbol{\sigma}$ requires an iterative procedure. The iterative scheme chosen here is the same in both methods used in the sequel, either in the FEM analysis or with the FFT-based method, and corresponds to the initial stiffness scheme. It can be written as follows:
At iterate $i+1$ of time-step t_{n+1}, $\boldsymbol{e}(u_n)$, $\boldsymbol{\sigma}_n$ and $\boldsymbol{e}(u^i)$ being known,

(a) Compute the elastic prediction $\boldsymbol{\sigma}^{E,i}$ with the help of (53), then the plastic correction $\boldsymbol{\sigma}^i$ with the help of (55).

(b) Convergence test: if the equilibrium condition is not met, go to (c). Otherwise set

$$\boldsymbol{e}(u_{n+1}) = \boldsymbol{e}(u^i), \quad \boldsymbol{\sigma}_{n+1} = \boldsymbol{\sigma}^i, \tag{56}$$

and exit.

(c) Solve the linear problem for $\delta u, \delta \boldsymbol{\sigma}$:

$$\left.\begin{array}{ll} \boldsymbol{\delta\sigma} = \mu \boldsymbol{e}(\delta u) + \boldsymbol{\sigma}^i, & \text{div}\boldsymbol{\delta\sigma} = 0, \\ \delta u \text{ periodic on } \partial Q, & \boldsymbol{\delta\sigma}.\boldsymbol{n} \text{ anti-periodic on } \partial Q. \end{array}\right\} \tag{57}$$

(d) Update $\boldsymbol{e}(u^i)$:

$$\boldsymbol{e}(u^{i+1}) = \boldsymbol{e}(u^i) + \boldsymbol{e}(\delta u). \tag{58}$$

FEM Analysis When the finite element method is used (laminates, section 5.2) the solution of the linear problem (57) is obtained classically after taking into account the periodicity condition to be satisfied by δu. This periodicity condition is imposed directly by an elimination technique as detailed in Michel *et al* [38], section 4.2. Regarding the convergence test on the equilibrium condition at step (b) of the iterative algorithm, it is met by ensuring that the relative norm of the maximum of the equilibrium residuals is less than a tolerance of 10^{-6}.

FFT-based method When the FFT method is used (complex microstructures, section 5.3) the solution of the linear problem (57) is obtained as detailed in Michel *et al* [38], section 5. Due to the uniformity of μ in the cell, this solution can be obtained without iterating. The Green's operator associated to μ takes the following expression in the Fourier space

$$\hat{\Gamma}_{ij}(\boldsymbol{\xi}) = \frac{\xi_i \xi_j}{\mu \left|\boldsymbol{\xi}\right|^2}. \tag{59}$$

The convergence test in step (b) of the iterative algorithm is on the relative norm of the maximum (in frequency) of the divergence of $\boldsymbol{\sigma}$ written in Fourier space with a tolerance of 10^{-4}.

5.2 Test example : laminates

Laminates are of interest for two reasons. First, they provide a sample example where exact results are available in (almost) closed form and which can be used to assess the accuracy of the computational procedure. Second, regarding the definition of the effective toughness of a composite material, they can be compared to with simulations performed by [27] where the propagation of the crack throughout the unit cell is followed.

The laminate consists of alternative layers of material 1 and material 2 (volume fraction $c^{(r)}$ and surface energy $\gamma^{(r)}$ in material r). For simplicity attention is restricted to dimension $d = 2$. The effective surface energy can be derived in closed form (see A for details). Laminates are anisotropic and the effective surface energy is expected to depend on the direction of propagation of the crack, or equivalently on the angle θ between the direction of propagation and the direction of layering. The polar diagram in figure 1 left shows the effective surface energy as a function of θ : when $\theta = 0$ the direction of propagation is parallel to the layers and the crack propagates in the weakest phase, $\gamma^{\text{hom}} = \text{Inf}(\gamma^{(1)}, \gamma^{(2)})$. When $\theta = \pi/2$, the crack propagates in the direction perpendicular to the layers, the shortest path is perpendicular to the layers in each layer and the effective surface energy is the average of the individual surface energies $\gamma^{\text{hom}} = c^{(1)}\gamma^{(1)} + c^{(2)}\gamma^{(2)}$. The domain shown in figure 1 right is the corresponding domain P^{hom} for the macroscopic "stress" (or "flow") $\boldsymbol{\Sigma} = (\Sigma_1, \Sigma_2)$ defined as

$$\Sigma_1 \leq \text{Inf}(\gamma^{(1)}, \gamma^{(2)}), \quad \text{and} \quad \Sigma_2 \leq c^{(1)}({\gamma^{(1)}}^2 - \Sigma_1^2)^{1/2} + c^{(2)}({\gamma^{(2)}}^2 - \Sigma_1^2)^{1/2}. \tag{60}$$

FEM analysis

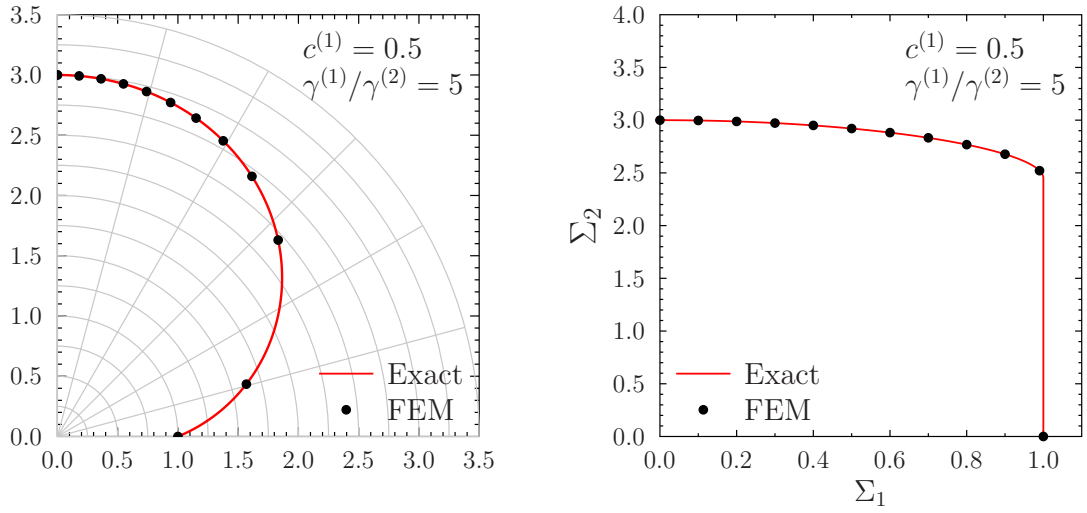

Figure 1: Laminates. Left: polar representation of the effective surface energy for a laminate as a function of the angle between the direction of lamination and the direction of propagation of the crack. Right: effective domain.

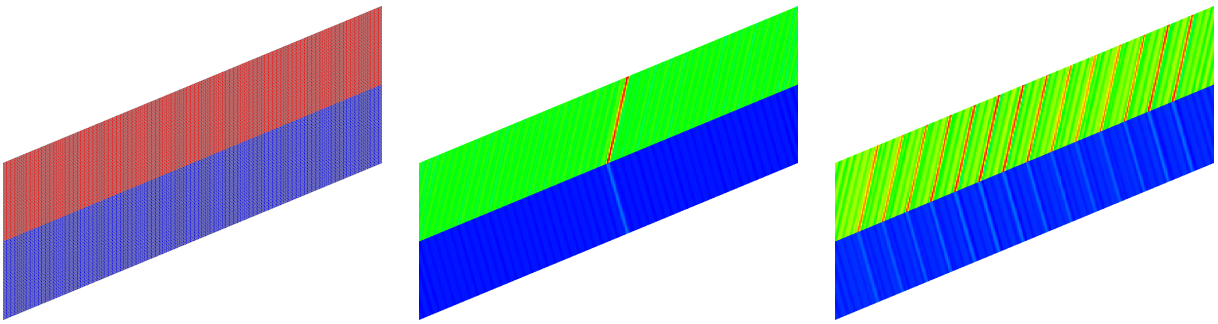

(a) (b) (c)

Figure 2: Laminate inclined at an angle $\theta = 3\pi/8$ on the direction $\boldsymbol{\nu} = \boldsymbol{e}_1$ (the normal to the crack path is horizontal in average). Different failure modes. (a) uniform gradient in each layer. (b) and (c) localized failure modes. Also shown in (a) is the mesh used in the FEM simulations.

The mesh used in the FEM simulations is shown in Figure 2a. It is a regular mesh consisting of 30456 quadratic 8-node elements and 92148 nodes in total. The mesh size is chosen to capture very localized failure modes. Computations were performed with $\gamma^{(1)} = 5\gamma^{(2)}$, $\mu = 10^3\gamma^{(2)}$. The time step is constant $\Delta t = 0.1\gamma^{(2)}/\mu$ (it takes 10 time steps to enter the "plastic" regime) and 1 000 time steps are performed to reach a limit state (average stress) with sufficient accuracy. Computations have been run on a laptop with less than 5 minutes CPU time on an Intel processor Core Xeon E-2176M.

The solid red line is the exact result (A), the dots are the results of the FEM analysis performed along the lines of paragraph 5.1 with the above algorithmic parameters. The agreement between the exact results and the computational results is seen to be excellent.

Minimizers (or failure modes)

Regarding the minimizers (or failure modes), as shown in A, a first and straightforward class of solutions to (53)-(55) consists of fields u with a uniform gradient parallel to the layers, and inhomogeneous in the direction perpendicular to the layers, with $\boldsymbol{\nabla} u$ being uniform in each layer. These solutions are found by the computational procedure when a uniform elastic modulus μ is used throughout the whole unit cell and when the initial condition for the time-stepping algorithm (52) is a uniform stress state (stress-free in our simulations).

A second class of solutions can be obtained analytically by considering discontinuous fields u, with discontinuities along straight lines (or plane surfaces in 3d) in each phase.

These lines are characterized by their inclination with respect to one of the coordinate axes. A deviation from uniformity has to be applied in the computational procedure to converge towards such discontinuous solutions. These defects are introduced in the (artificial) elastic modulus by assigning a weaker modulus $\mu^w = 3/4\mu$ to a pair of elements located face-to-face across the interface between the layers (or to multiple pairs of such elements in the case of multiple strain localization lines).

Both classes of solutions give the same average stress and the same effective surface energy. However, this example illustrates the fact that the unit-cell problem may have several solutions (infinitely many solutions actually) and that not all of them are minimum cuts of the unit cell. The multiplicity of the solutions is illustrated in figure 2. The layers are inclined on the horizontal axis at an angle $\pi/8$ and the vector $\boldsymbol{\nu}$ normal (in average) to the crack direction is horizontal (hence the angle θ between $\boldsymbol{\nu}$ and the vertical direction is $3\pi/8$). The "crack" propagates in average in the vertical direction. The minimizers u can be either fields with uniform gradient in each layer, or fields with localized gradient along lines with a specific orientation. Single lines as well as multiple lines are possible solutions.

5.3 Particle-reinforced materials

In this section, two or three-dimensional microstructures made of a matrix containing tougher inclusions are considered. All numerical simulations in this section have been performed using the iterative FFT numerical scheme described in section 5.1 above and implemented in an in-house code parallelized with OpenMP. All the simulations were performed using the same algorithmic parameters as those already used in the laminate test example, namely $\mu = 10^3\gamma^{(2)}$ now noting $\gamma^{(2)}$ the surface energy of the matrix material and 1000 time steps of $\Delta t = 0.1\gamma^{(2)}/\mu$ for the limit state. Regarding the computation times that will be mentioned in the following, they have been obtained on a computer with 512 GB DDR4 RAM and two Intel Xeon Gold 6154 3 GHz processors (36 cores in total).

5.3.1 Circular or spherical inclusions

In this section we consider two and three-dimensional microstructures consisting of a matrix containing tougher inclusions, either circular (2d) or spherical (3d) with different sizes at different volume fractions of inclusions. The Hashin-Shtrikman bound (47) provides a rather accurate approximation of the overall shear modulus of a matrix (phase 2) reinforced by circular or spherical inclusions (phase 1) and can be used to estimate the variational upper bound of section 4.

In dimension $d = 2$, the configurations which were investigated contained 992 inclusions of different sizes. More specifically 5 populations of circular disks were considered with radius 1 (512 disks), 2 (256 disks), 3 (128 disks), 4 (64 disks), 5 (32 disks) respectively. The spatial resolution of the image is 6561^2 pixels. A rather high volume fraction of inclusions was used ($c^{(1)} = 0.8$) with the hope to achieve a significant increase in the surface energy. To achieve this rather high volume fraction a specific code due to Donev [15] was used. The crack propagates in average in the vertical direction ($\boldsymbol{\nu}$ is horizontal). Simulations were performed for 6 different values of the phase surface energy contrast: $\gamma^{(1)}/\gamma^{(2)} = 1.0625, 1.125, 1.25, 1.5, 2$ and 3 with $\gamma^{(1)}$ the surface energy in the inclusions and $\gamma^{(2)}$ the surface energy in the matrix. As an indication, the CPU time ranges from about 6 hours when $\gamma^{(1)}/\gamma^{(2)} = 1.0625$ to about 15 hours when $\gamma^{(1)}/\gamma^{(2)} = 3$.

The shortest paths (weighted by the surface energy of the individual phases) are shown in figure 3 for two different values of the contrast $\gamma^{(1)}/\gamma^{(2)} = 1.125$ and 1.5. The shortest paths found by the computational method have several branches, although probably a single branch would suffice. At the lowest contrast (snapshot in the middle in figure 3), a few inclusions are cut (the path cutting through the inclusions is shown in green whereas it is shown in red in the matrix). At the highest contrast, the path is entirely contained in the matrix and the inclusions play no role. This explains why increasing the surface energy in the inclusions does not improve the effective surface energy.

In 3d, a distribution of 93 spheres with 3 groups of different sizes was used in the simulations (73 small, 12 medium, and 8 large inclusions, the size ratios with respect to the smallest size being respectively 1.0, 1.8, and 3.5). The volume fraction of inclusions is $c^{(1)} = 0.65$. Donev's code [15] was used again to generate this three-dimensional distribution. The inclusion phase is shown in figure 4 middle. The spatial resolution of the image is 243^3 voxels. As in the previous case of two-dimensional microstructures, simulations were conducted for 6 values of the contrast $\gamma^{(1)}/\gamma^{(2)} = 1.0625, 1.125, 1.25, 1.5, 2$ and 3. The CPU times were of the order of 30 minutes when $\gamma^{(1)}/\gamma^{(2)} = 1.0625$ to 1h30 when $\gamma^{(1)}/\gamma^{(2)} = 3$.

Although the inclusions seem to be densely packed, the algorithm finds a rather flat minimum cut surface shown on the right (contrast = 3). The surface avoids all inclusions and lies entirely in the matrix. In both cases (2d and 3d microstructures) the simulations and the variational bound show the same trends, first an increase of the effective surface energy as the contrast increases followed by a plateau which is reached for a finite value of the contrast. Above this threshold, no increase of the effective surface energy is expected. Although the trends are similar, the toughening effect of the inclusions is rather low in the simulations, significantly lower than the predictions of the variational upper bound and much lower than the rule of mixtures (Voigt bound).

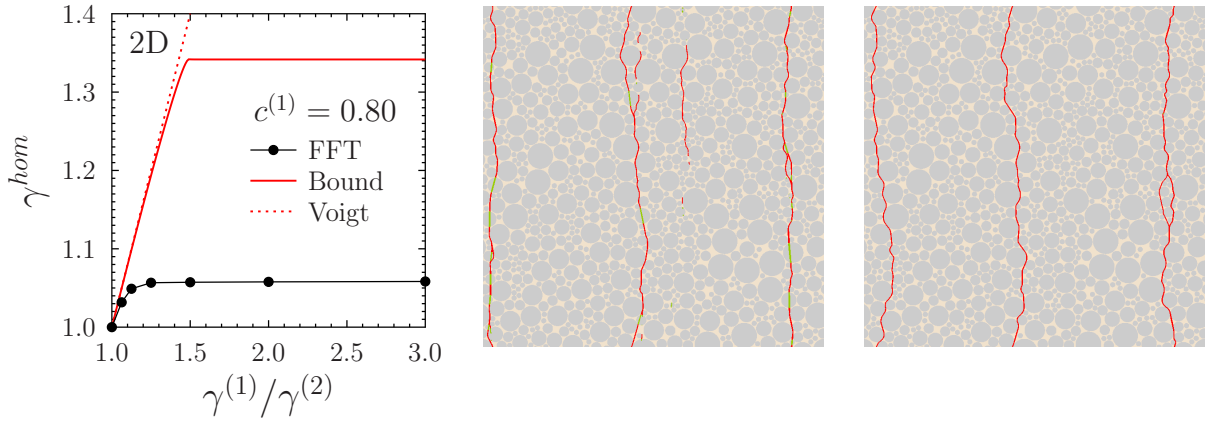

Figure 3: Two-dimensional particulate composite containing circular inclusions (microstructure shown on the snapshots on the right). Volume fraction $c^{(1)} = 0.8$. Left: effective surface energy as a function of the contrast. Middle and right: minimum cuts (red in the matrix, green in the inclusions). Middle, contrast = 1.125 (note that a few particles are cut). Right: contrast = 1.5 (the cut is entirely in the matrix).

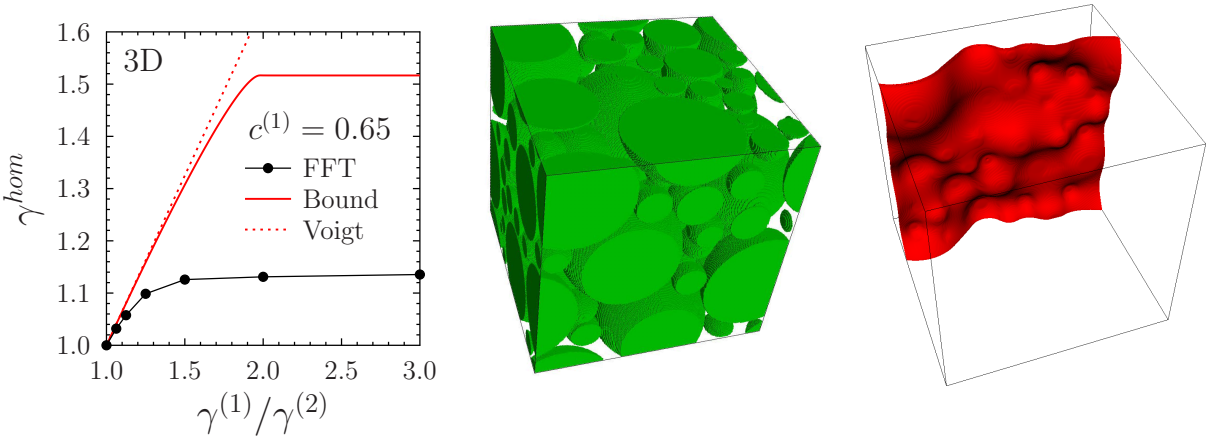

Figure 4: Three-dimensional matrix (phase 2) containing a population of polydisperse spherical inclusions (phase 1) with volume fraction $c^{(1)} = 0.65$. Left: effective surface energy as a function of the contrast. Middle: microstructure (only the inclusions are shown for clarity). Right: minimum cut with a contrast $\gamma^{(1)}/\gamma^{(2)} = 3$.

5.3.2 Elongated particles

In an attempt to increase the area of the minimum cuts and therefore the toughening effect, simulations were performed with elongated particles. More specifically microstructures containing 100 ellipsoids with volume fraction $c^{(1)} = 0.3$, aspect ratio $=$ 10, identical in size but randomly oriented and randomly placed with the only constraint of non-interprenetration, were generated by means of the code of Donev [15]. A typical microstructure is shown in figure 5 (top left) and the corresponding effective surface energy as a function of the contrast is plotted on the top row right. The spatial resolution of the images is 675^3. The simulations were conducted for 5 values of the contrast $\gamma^{(1)}/\gamma^{(2)} = 2, 5, 10, 15$ and 20. The CPU times range from about 24 hours when $\gamma^{(1)}/\gamma^{(2)} = 2$ to 3 days when $\gamma^{(1)}/\gamma^{(2)} = 20$.

The minimum cuts for two contrast $\gamma^{(1)}/\gamma^{(2)} = 2$ and 20 respectively are shown in the bottom row. Note that for the lowest contrast (=2) several particles are cut, whereas none is cut at the largest contrast (20).

6 Discussion: effective toughness of heterogeneous materials

The question addressed in this section is the following: *can the effective surface energy studied in the previous sections be considered as the actual "effective fracture energy" of the composite material as initially proposed by Schneider [45] under the name of "effective crack resistance"?*

There are many advantages to the variational characterization of this effective energy that we summarize briefly. First of all, its definition is mathematically indisputable. Second it can be determined with a relatively simple computational strategy using the analogy with limit loads. Third it opens the way to the derivation of bounds which have proven their interest for other physical properties of composite materials . However adopting this definition as the "effective fracture energy" is challenged by simple physical intuition (which of course should be used with care) and by existing results on the propagation of a crack in a heterogeneous material. Here are some of the objections:

1. It results from the most elementary variational bound (41) that the effective surface energy cannot exceed the rule of mixtures (average of the toughnesses of the phases). Unfortunately there are situations where the effective toughness (in a sense which remains to be specified) exceeds this "rule" (an example will be provided in section 6.1).

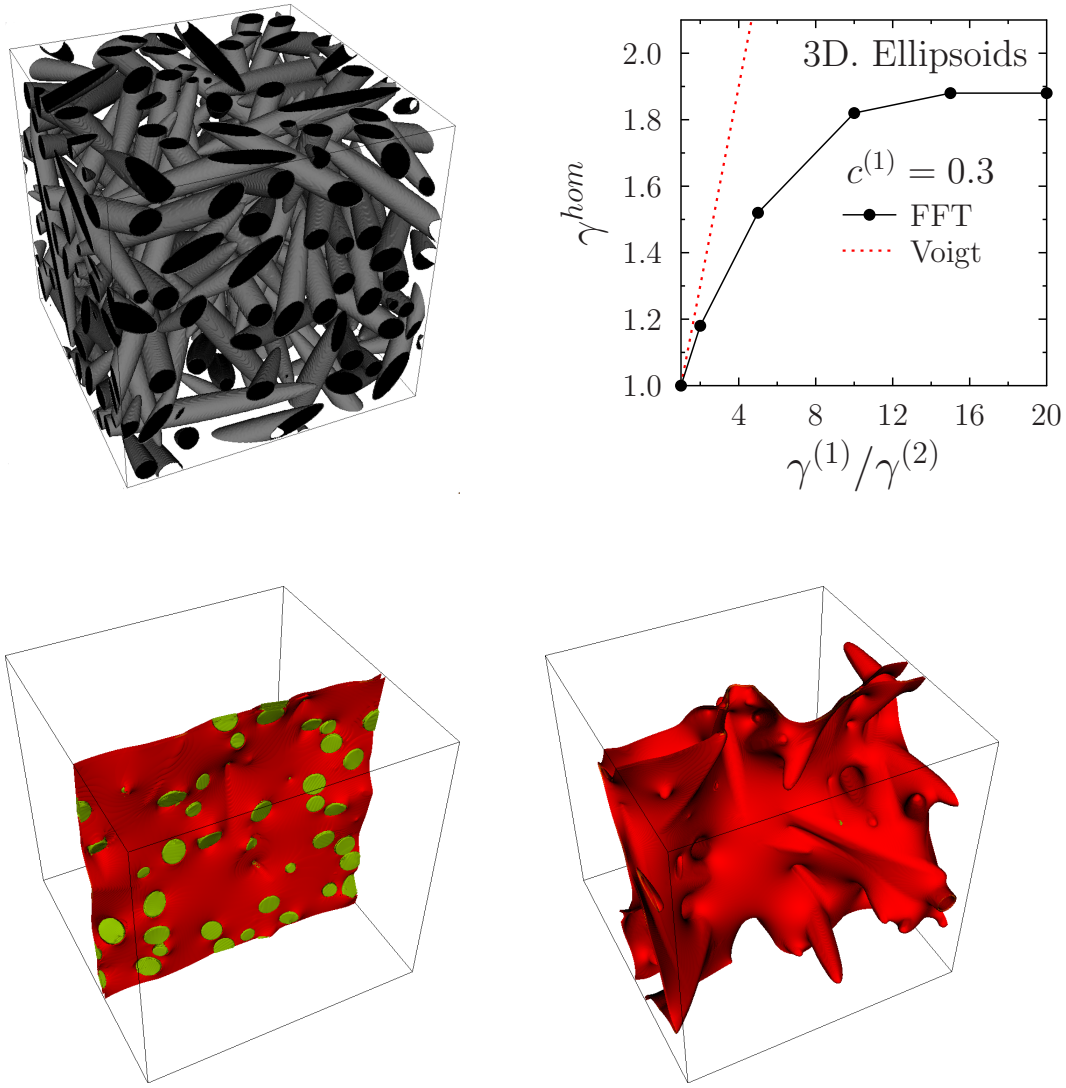

Figure 5: Ellipsoidal inclusions. Aspect ratio = 10, volume fraction $c^{(1)} = 0.3$. Top left: typical microstructure. Top right: effective surface energy as a function of the contrast. Bottom: minimum cuts. minimum cuts are shown in red in the matrix and in green in the inclusions. Bottom left : contrast $\gamma^{(1)}/\gamma^{(2)} = 2$ (note that several inclusions are cut). Bottom right : contrast $\gamma^{(1)}/\gamma^{(2)} = 20$ (note that no inclusion is cut).

2. The effective surface energy does not depend on the elastic properties of the phases and is in fact totally decorrelated from it. This is a direct consequence of the mathematical results of section 2. However numerical simulations (Hossain *et al* [27]) as well as theoretical arguments show that the effective toughness of the composite may depend on the elastic contrast between the two phases (the same simple example in section 6.1 will again confirm this dependence).

Before adressing these points, let us note that a proper mathematical definition of the "effective fracture energy" of a heterogeneous material is still lacking. It is therefore not surprizing that different authors, using different definitions, arrive at different results. In a recent study Lebihain *et al* [31] identified three possible definitions in the literature, which we recall now. They simulate the propagation of a crack through an array of obstacles, assuming that this crack remains macroscopically coplanar. They assume that the crack evolution is governed by the energy release rate (ERR) G of the specimen and that the crack propagates when the local ERR reaches a critical value. They compute the local ERR either numerically or estimate it theoretically through the stress intensity factors at the crack tip using a perturbation technique. The local velocity of the front crack is governed by a specific propagation criterion (orientation and velocity) where the ERR may exceed the fracture energy G_c and therefore departs from the original Griffith's law. Although their study is not based on the variational approach of fracture that was used from the true beginning of the present work, some of their conclusions are meaningful in the present context. Here are the three possible definitions which they identified:

1. the average (in time) of the total energy dissipated by the fracture process, which is the definition of the effective fracture energy given in the introduction and that we adopt here as a the most physical definition,

2. the average (in time and space) of the ERR along the front during crack propagation,

3. the maximum (in time and space) ERR during crack propagation.

Lebihain *et al* show that the first two definitions are equivalent, but that a length-scale separation has to hold in order for the third definition to coincide with the two others (clearly the third definition leads to a larger value of the effective fracture energy than the two others). This third definition is the one used in the simulations of Hossain *et al* [27] and Brach *et al* [8]. It should however be noted that when considering only the maximum value of the ERR in time, nothing is said about the advance of the crack after the peak and in-between the peaks of the ERR. It is not clear that the assumption of a quasi-static evolution that prevails before the peak remains valid after the peak. Significant inertia effects might develop after the peak as suggested for instance in [29]. Regarding the

average in time of the ERR (second definition above), the problem is highly reminiscent of that of systems governed by wiggly energies (Menon [36]) and should be considered in that framework. This is beyond the scope of the present paper.

The definition which is closest to the variational characterization (16) of the effective surface energy (*i.e.,* Schneider's definition of the effective fracture energy) is the first one based on the energy dissipation. There is however a significant difference: the present effective surface energy (16) disregards the propagation stage of the crack. It is the minimum energy dissipated along *every possible path*, whereas the first definition above is the energy dissipated along the *actual* path followed by a pre-existing crack. So Schneider's variational definition of the effective fracture energy is indeed different from the three definitions above.

6.1 A simple, but instructive, example

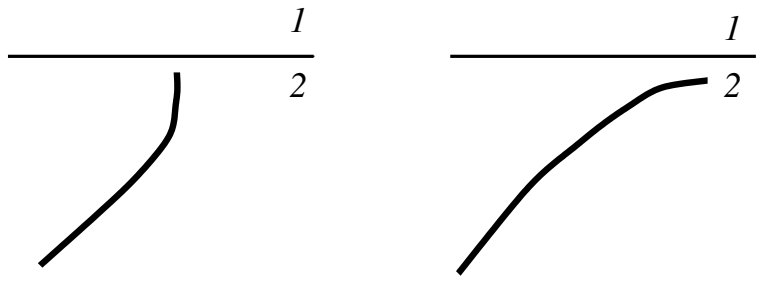

Figure 6: Deviation of a crack approaching an interface between two materials with different elastic moduli (after He & Hutchinson [26]). Left: material 1 stiffer than material 2. Right: material 1 more compliant than material 2.

To get a better understanding of the limitations of the variational definition of the effective toughness, let us consider the simple situation of a laminate where the two phases have the same toughness but different elastic moduli. It has been shown, first in a seminal paper by He and Hutchinson [26] on layered materials, confirmed by Hsueh *et al* [28] and Brach *et al* [8] by numerical simulation, that a crack may deviate at the interface between two elastically different materials. Consider the simple case where both phases have the same toughness but different elastic moduli. The effective surface energy given by the variational characterization (17) is the same as that of the phases. However, when one follows the propagation, the elastic stress field at the crack tip is perturbed when the

crack approaches the elastic heterogeneity and the crack may deviate from a straight line (minimum cut).

Consider now a laminated material. According to the above remark, any crack in this laminate (irrespective of its initial location), will meander from one layer to the next one, whereas the crack path predicted by the variational definition (16) is a straight line (the fracture energy being the same in all phases). The energy dissipated along the crack propagation does not depend on where the crack is formed initially, as the problem is invariant by translation along the layers, and it depends only on $\boldsymbol{\nu}$. Two lessons can be learned from this simple example.

1. First the effective toughness (in the sense of the energy dissipated along the actual crack path) can exceed the rule of mixtures (in the present case, since both materials have the same toughness, the rule of mixtures is this common value). This violation of the rule of mixtures is indeed consistent with other authors' results. Indeed, Hsueh *et al* [28] report that incorporating a more compliant phase in a given material (both phases having a similar toughness) might lead to a significant increase in fracture toughness for the mixture through the pinning of the crack by the compliant phase.

2. Second, the toughness of a homogeneous material can be enhanced by spatially modulating its stiffness. The use of more compliant inclusions is indeed well-known in the materials science literature (see Bagheri *et al* [2] for a review on the mechanisms at play in rubber-toughened epoxies). It is also used in Brodnik *et al* [11] to design a microstructure capable of enhancing the toughness of a material. Interestingly, the effective fracture energy often *increases* when the elasticity of the compliant phase *is decreased*. Unfortunately for the variational definition of the effective fracture energy, it does not capture the role of the relative stiffness of the phases.

6.2 On the bounding character of the variational definition of the effective toughness

Despite the above criticisms, it is interesting to note that the effective surface energy has a rigorous bounding character for the effective fracture energy of a composite material. Indeed, (16) focuses on the *worst-case scenario*, *i.e.*, the crack configuration delivering the smallest possible dissipation, irrespective of the fact that this configuration corresponds, or not, to the surface followed by an actual crack. By contrast, the average fracture energy mentioned in definition 1 above corresponds to the dissipation along the propagation of an actual crack, which may depend on the initial location of the crack. This crack configuration is a possible trial configuration in the variational principle (16). But since

it is not necessarily optimal, the effective surface energy (16) is a rigorous *lower bound* to the average fracture energy dissipated along the actual fracture process (definition 1) and *a fortiori* a lower bound to the "effective toughness" based on the third definition (ERR max).

The variational principle (16) leads therefore to a fourth possible definition of the effective toughness that could be called "variational fracture energy" or "worst-case fracture energy"). It is indeed safer than the three other ones, although it is unlikely to be observed at least when the phases have different elastic moduli. It does not account for the contrast in elastic properties of the phases and this is certainly a limitation of this definition, as the above example shows.

When designing a structure for improved toughness, choosing the worst-case scenario is certainly the safest option. However, it deprives the designer of the possibility of playing with the elastic contrast between the phases. It may also be too pessimistic, since as remark 7 in section 4 shows, when no information about the microstructure is available besides its isotropy, then the worst-case scenario is the Reuss bound and it is attained (and shows no toughening of the material). To be consistent with the lower bound character of the variational definition, designing a microstructure for enhanced toughness based on this definition would require to develop accurate *lower* bounds for the effective surface energy γ^{hom}, incorporating additional microstructural information to improve on the Reuss bound, which is a highly difficult task and has been virtually untouched.

Interestingly, the variational bounds of section 4 which are upper bound to the worst case, can be compared in figure 7 with the numerical simulations of Lebihain *et al* [31] where the propagation of a crack through a random distribution of spherical inclusions is simulated using a perturbative approach with no elastic contrast between the inclusion and the matrix. Although the definition of the effective toughness adopted in [31] is slightly different from the effective surface energy studied here (energy dissipated along the actual crack path), it is interesting to observe that the predictions of the bounds are in good agreement with the simulations, both qualitatively (the threshold of the contrast over which there is no further toughening of the composite) and quantitatively. To be fully honest there is a bit of luck, or error compensation, in this good agreement, since one the one hand the variational effective toughness (16) is a lower bound to the effective toughness and on the other hand the bound (50) is an upper bound to this lower bound.

6.3 What is missing?

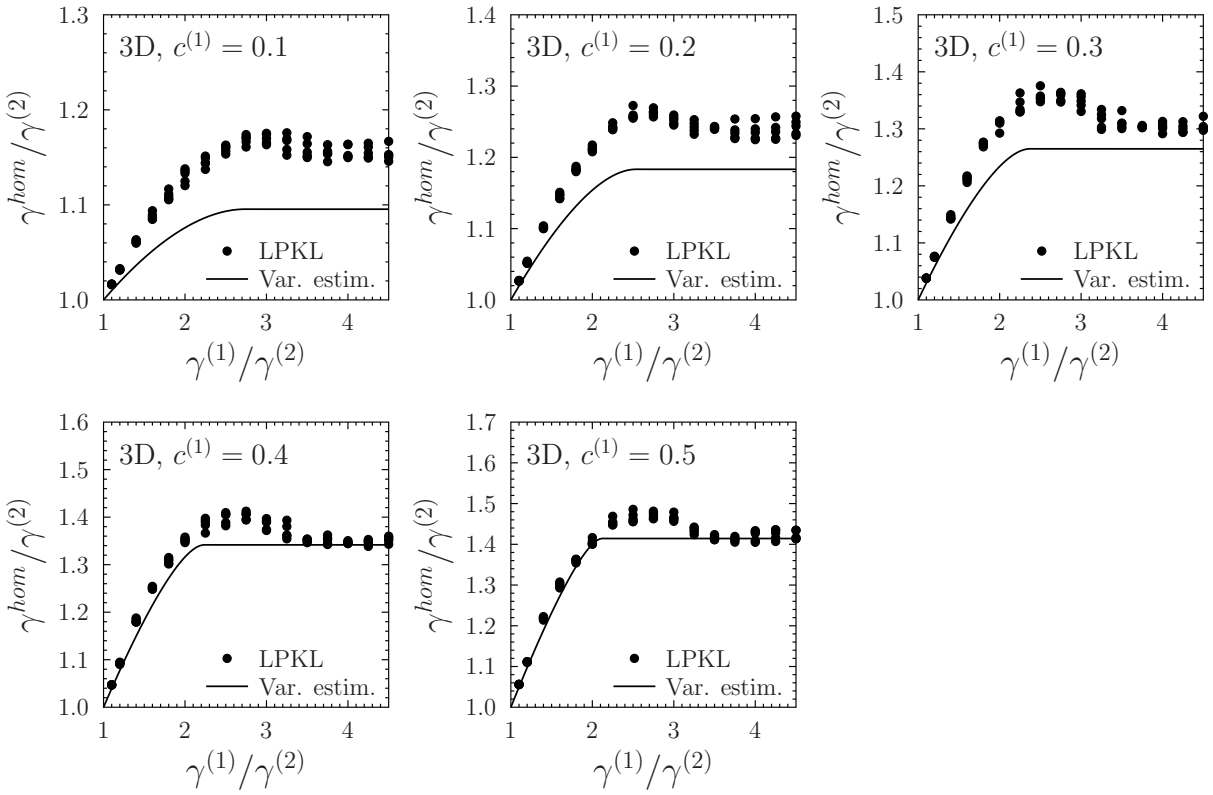

Figure 7: Effective surface energy for a particulate composite reinforced by spherical inclusions. Circles: simulations by Lebihain *et al* [31] (LPKL). Solid lines: variational estimate (50)-(51).

We review here a few assumptions that have been made to arrive at the variational definition of the effective fracture energy and which are disputable. First of all, the assumption of a quasi-static evolution has been made from the true beginning and throughout this study. It is not clear whether the crack propagation in a heterogeneous material can be considered as quasi-static, or if inertia effects have to be taken into account. Significant differences due to dynamic effects (versus quasi-static evolution) are reported in Lazzaroni *et al* [29].

The remainder of this discussion assumes that the assumption of a quasi-static evolution is legitimate. Even within this assumption, a certain number of simplifications have been made to arrive at the variational definition (16) of the effective fracture energy. As already mentioned, it does not account in details for the crack propagation and in particular it is *not* formulated as a time evolution process. This is quite surprising since the variational model of fracture (1) which is the starting point of the formulation has been precisely designed to study the evolution in time of a crack. So one can wonder where this information was lost. Three possible origins for this loss are discussed below as possible ways of improvement for the variational definition. All the developments of section 2 are mathematically rigorous so the loss of information is in the transition between the initial variational model of fracture (1) and the variational homogenization problem (3). This transition should be examined with more care.

First, the notion of "the past" has been lost in the transition between (2) and (3) when the irreversibility condition $\Gamma \supset \Gamma_n$ has been left aside. Situations where the crack is pinned by tougher inclusions, and remains so, are therefore disregarded by removing the irreversibility constraint on Γ. In order to remain as close as possible to the definitions of the effective toughness based on crack propagation, the homogenization problem should take into account the irreversibility condition. This was done by Giacomini and Ponsiglione [25] in the scalar setting (u is a scalar field) who confirmed the decoupling between the bulk and the surface energy after homogenization. Even though the extension to elasticity remains to be done, it is unlikely that the outcome will be very different from the scalar case.

The second weak point in the simplifications leading to (3) is the consideration of nucleation with an energy in the form (1). Indeed the mention of pinning of a crack brings symmetrically the question of its unpinning. By unpinning it is meant that the crack could be trapped in some location and that another ingredient would be needed to reactivate it. One could think for instance of a crack propagating in a matrix containing an array of circular holes. It is likely that this crack will eventually be attracted to one of the holes and may get trapped in it. In order to generate a new crack, either from this location or from another one, crack nucleation has to be made possible by the model. Unfortunately

the homogenization results of section 2 hold for energies in the form (4) or (1) and it is known that the energy (1) fails to predict nucleation of cracks properly. As pointed out in Tanné *et al* [54] predicting nucleation requires a regularized energy corresponding to a model incorporating the gradient of damage variables (sometimes called a phase-field model) with a fixed characteristic length ℓ_{ch} depending on the critical stress and on the toughness of the material. Hossain *et al* [27] used such a phase-field model in their simulations. But this regularized model raises two questions: first, its homogenization has to be explored and second the interplay between the (fixed) characteristic length ℓ_{ch} and the size of the unit cells ε has to be investigated. As Tanné *et al* report, when the heterogeneities are smaller that the characteristic length, they become invisible to the phase field model.

A third question which arises is the interplay between the time-discretization and the size of the microstructure. Before homogenization, the time-discretized problem (2) contains two small parameters, the time step Δt and the size of the microstructure measured by ε. There are many examples of situations where the limits as these two parameters tend to 0 do not commute. In the present study, the time step is considered as large with respect to the size of the unit cell, whereas when simulating the propagation of a crack in the unit cell (as in [27, 31]), the time-step is "small" with respect to the size of the heterogeneities and it takes a finite time to break the unit cell. Of course the comparison between a time scale and a length scale does not make sense unless it is performed relative to a velocity, that of the crack or of the elastic waves, but what is meant is that in the approaches where the crack propagation is simulated step-by-step it takes an infinite number of time steps (in practice a large number) for the crack to break the unit cell. Therefore the interplay between the two small parameters deserves to be explored in more details.

7 Conclusion

The variational definition of the effective toughness of a composite material proposed by Schneider based on rigorous mathematical results, has been assessed. Similarities with plasticity and with limit loads have been highlighted and have been used both in numerical simulations and in the derivation of (upper) bounds for the effective surface energy.

The variational definition has merits and limits:

- In favor of it, is his rigorous mathematical definition and its indisputable lower bound character.
- It has nevertheless a few limitations by comparison with a physically-based definition which is the energy dissipated along the actual crack propagation. First, it shows

no influence of the difference in elastic moduli of the constituents whereas both numerical simulations and simple examples show that there should be an influence of the elastic heterogeneity. This limitation deprives the designer to use the elastic contrast as a toughening mechanisms. Second, according to this definition, the effective toughness of a composite material should never exceed the average of the toughness of the phases. Again this is at odds with simple examples and earlier work where it was noticed that the rule of mixtures could be exceeded.

In conclusion, the variational definition of the effective toughness is, at present, the only one with solid mathematical foundations. However, it should be improved to account for physical features and in particular its coupling with the elastic properties of the phases.

Acknowledments: The authors are indebted to M. Lebihain for kindly providing the numerical results from [31] used in figure 7 for comparison with the variational estimates. The authors are also grateful to the reviewers whose comments and suggestions greatly helped in improving the manuscript. It should also be said that when the authors submitted the initial version of the manuscript they were unaware of the recent work of Ernesti and Schneider [17] who contains some of the suggestions of section 6. We chose to maintain the discussion for consistency, but we acknowledge the existence of this independent work.

References

[1] E. Anderheggen and H. Knöpfel. Finite element limit analysis using linear programming. *International Journal of Solids and Structures*, **8** (12):1413–1431, 1972.

[2] R. Bagheri, B. Marouf, and R. Pearson. Rubber-toughened epoxies: A critical review. *Polymer Reviews*, 49:201–225, 07 2009.

[3] G. Bouchitté. Convergence et relaxation de fonctionnelles du calcul des variations à croissance linéaire. *Annales de la Faculté des Sciences de Toulouse*, **8**:7–36, 1986-1987.

[4] G. Bouchitté, I. Fonseca, and L. Mascarenhas. A global method for relaxation. *Archive for Rational Mechanics and Analysis*, **145**(1):51–98, 1998.

[5] G. Bouchitté and P. Suquet. Homogenization, Plasticity and Yield design. In G. Dal Maso and G.F. Dell'Antonio, editors, *Composite Media and Homogenization Theory*, pages 107–133. Birkhaüser, Boston, 1991.

[6] B. Bourdin, G.A. Francfort, and J.-J. Marigo. The variational approach to fracture. *Journal of Elasticity*, **91**: 5–148, 2008.

[7] A. Bower and M. Ortiz. A three dimensional analysis of crack trapping and bridging by tough particles. *Journal of the Mechanics and Physics of Solids*, **39**: 815–858, 1991.

[8] S. Brach, M.Z. Hossain, B. Bourdin, and K. Bhattacharya. Anisotropy of the effective toughness of layered media. *Journal of the Mechanics and Physics of Solids*, **131**:96 – 111, 2019.

[9] A. Braides and V. Chiadò Piat. A derivation formula for convex functionals defined on $BV(\Omega)$. *Journal of Convex Analysis*, **2**:69–85, 1995.

[10] A. Braides, A. Defranceschi, and E. Vitali. Homogenization of free discontinuity problems. *Archive for Rational Mechanics and Analysis*, **135**:297–356, 1996.

[11] N. Brodnik, C.-J. Hsueh, K. Faber, B. Bourdin, G. Ravichandran, and K. Bhattacharya. Guiding and Trapping Cracks With Compliant Inclusions for Enhancing Toughness of Brittle Composite Materials. *Journal Applied Mechanics*, **87**:031018–1–031018–10, 2020.

[12] A. Chambolle and G. Thouroude. Plane-like minimizers in periodic media: the cell problem. In Scuola Normale Superiore, editor, *Singularities in nonlinear evolution phenomena and applications*, pages 89–106, 2009.

[13] E. Christiansen. Computations of limit loads. *International Journal for Numerical Methods in Engineering*, **17**:1547–1570, 1981.

[14] V. Crismale, M. Friedrich, and F. Solombrino. Integral representation for energies in linear elasticity with surface discontinuities. *Advances in Calculus of Variations*, page 000010151520200047, 2020.

[15] A. Donev, F. H. Stillinger, and S. Torquato. Neighbor List Collision-Driven Molecular Dynamics Simulation for Nonspherical Particles. I. Algorithmic Details II. Applications to Ellipses and Ellipsoids. *Journal of Computational Physics*, **202**:737–764 (part I) and 765–793 (part II), 2005. see also https://cims.nyu.edu/ donev/Packing/PackLSD/Instructions.html.

[16] D. C. Drucker, W. Prager, and H. J. Greenberg. Extended limit design theorems for continuous media. *Quarterly of Applied Mathematics*, **9**(4):381–389, 1952.

[17] F. Ernesti and M. Schneider. A Fast Fourier transform based method for computing the effective crack energy of a heterogeneous material on a combinatorially consistent grid. *International Journal of Numerical Methods in Engineering*, **122**:1–25, 2021.

[18] F. Ernesti and M. Schneider. Computing the effective crack energy of heterogeneous and anisotropic microstructures via anisotropic minimal surfaces. *Computational Mechanics*, **69**, 2022.

[19] G.A. Francfort and J.J. Marigo. Revisiting brittle fracture as an energy minimization problem. *Journal of the Mechanics and Physics of Solids*, **46**:1319–1342, 1998.

[20] M. Friedrich, M. Perugini, and F. Solombrino. Γ-convergence for free-discontinuity problems in linear elasticity: Homogenization and relaxation. *Indiana University Mathematics Journal*, 2020. https://arxiv.org/abs/2010.05461.

[21] D. Gabay and B. Mercier. A dual algorithm for the solution of nonlinear variational problems via Finite Element approximation. *Computers and Mathematics with Applications*, **2**:17–40, 1976.

[22] H. Gao and J. Rice. A first order perturbation analysis of crack trapping by arrays of obstacles. *Journal of Applied Mechanics*, **56**:838–836, 1989.

[23] Y. Gao. Fracture analysis of nonhomogeneous materials via a moduli-perturbation approach. *International Journal of Solids and Structures*, **27**:1663–1682, 1991.

[24] A. Garroni, V. Nesi, and M. Ponsiglione. Dieletric breakdown: optimal bounds. *Proc. R. Soc. London A*, **457**:2317–2335, 2001.

[25] A. Giacomini and M. Ponsiglione. A Γ-convergence approach to stability of unilateral minimality properties in fracture mechanics and applications. *Archive for Rational Mechanics and Analysis*, **180**:399–447, 2006.

[26] M.Y. He and J.W. Hutchinson. Crack deflection at an interface between dissimilar elastic materials. *International Journal of Solids and Structures*, **25**:1053–1067, 1989.

[27] M.Z. Hossain, C.-J. Hsueh, B. Bourdin, and K. Bhattacharya. Effective toughness of heterogeneous media. *Journal of the Mechanics and Physics of Solids*, **71**:15 – 32, 2014.

[28] C-J. Hsueh, L. Avellar, B. Bourdin, G. Ravichandran, and K. Bhattacharya. Stress fluctuation, crack renucleation and toughening in layered materials. *Journal of the*

Mechanics and Physics of Solids, **120**:68–78, 2018. Special issue in honor of Ares J. Rosakis on the occasion of his 60th birthday.

[29] G. Lazzaroni, R. Bargellini, P.-E. Dumouchel, and J.-J. Marigo. On the role of kinetic energy during unstable propagation in a heterogeneous peeling test. *International Journal of Fracture*, **175** :127–150, 2012.

[30] M. Lebihain, J.-B. Leblond, and L. Ponson. Effective toughness of periodic heterogeneous materials: the effect of out-of-plane excursions of cracks. *Journal of the Mechanics and Physics of Solids*, **137**:103876, 2020.

[31] M. Lebihain, L. Ponson, D. Kondo, and J.-B. Leblond. Effective toughness of disordered brittle solids: A homogenization framework. *Journal of the Mechanics and Physics of Solids*, **153**:104463, 2021.

[32] K. Madou and J.B. Leblond. A Gurson-type criterion for porous ductile solids containing arbitrary ellipsoidal voids: II Determination of yield criterion parameters. *Journal of the Mechanics and Physics of Solids*, **60**:1037–1058, 2012.

[33] P. Marcellini. Periodic solutions and homogenization of nonlinear variational problems. *Annali di Matematica Pura ed Applicata*, **117**:139–152, 1978.

[34] J.J. Marigo, P. Mialon, J.C. Michel, and P.Suquet. Plasticité et homogénéisation : un exemple de prévision des charges limites d'une structure périodiquement hétérogène. *Journal de Mécanique Théorique et Appliquée*, **6**:47–75, 1987.

[35] H. Matthies, G. Strang, and E. Christiansen. The saddle point of a differential program. In R. Glowinski, E.V. Rodin, and O.C. Zienckiewicz, editors, *Energy methods in Finite Element analysis*, pages 309–318. Wiley, New-York, 1979.

[36] G. Menon. Gradient Systems with Wiggly Energies and Related Averaging Problems. *Archive for Rational Mechanics and Analysis*, **162**:193-246, 2002.

[37] B. Mercier. Une méthode de résolution du problème des charges limites utilisant les fluides de Bingham. *Comptes Rendus Académie des Sciences Paris, A*, **281**:525–527, 1975.

[38] J.-C. Michel, H. Moulinec, and P. Suquet. Effective properties of composite materials with periodic microstructure: a computational approach. *Computer Methods in Applied Mechanics and Engineering*, **172**:109–143, 1999.

[39] T. Mower and A. Argon. Experimental investigations of crack trapping in brittle heterogeneous solids. *Mechanics of Materials*, **19**:343–364, 1995.

[40] S. Müller. Homogenization of nonconvex integral functionals and cellular elastic materials. *Archive for Rational Mechanics and Analysis*, **99**:189–212, 1987.

[41] P. Ponte Castañeda. New variational principles in plasticity and their application to composite materials. *Journal of the Mechanics and Physics of Solids*, **40**:1757–1788, 1992.

[42] P. Ponte Castañeda and P. Suquet. Nonlinear composites. In E. Van der Giessen and T.Y. Wu, editors, *Advances in Applied Mechanics*, volume **34**, pages 171–302. Academic Press, New York, 1997.

[43] S. Roux, D. Vandembroucq, and F. Hild. Effective toughness of heterogeneous brittle materials. *European Journal of Mechanics - A/Solids*, **22**:743–749, 2005.

[44] J. Salençon. *Yield Design*. ISTE. John Wiley, 2013.

[45] M. Schneider. An FFT-based method for computing weighted minimal surfaces in microstructures with applications to the computational homogenization of brittle fracture. *International Journal for Numerical Methods in Engineering*, **121**:1367–1387, 2020.

[46] S.W. Sloan and P.W. Kleeman. Upper bound limit analysis using discontinuous velocity fields. *Computer Methods in Applied Mechanics and Engineering*, **127**(1):293–314, 1995.

[47] G. Strang. Maximal flow through a domain. *Mathematical Programming*, **26**:123–143, 1983.

[48] G. Strang. Maximum flows and minimum cuts in the plane. *Journal of Global Optimization*, **47**:527–535, 2010.

[49] P. Suquet. Local and global aspects in the mathematical theory of plasticity. In A. Sawczuk and G. Bianchi, editors, *Plasticity Today: Modelling, Methods and Applications*, pages 279–310, London, 1985. Elsevier.

[50] P. Suquet. Elements of Homogenization for Inelastic Solid Mechanics. In E. Sanchez-Palencia and A. Zaoui, editors, *Homogenization Techniques for Composite Media*, volume **272** of *Lecture Notes in Physics*, pages 193–278, New York, 1987. Springer Verlag.

[51] P. Suquet. Overall potentials and extremal surfaces of power law or ideally plastic materials. *Journal of the Mechanics and Physics of Solids*, **41**:981–1002, 1993.

[52] P. Suquet. Overall properties of nonlinear composites : a modified secant moduli theory and its link with Ponte Castañeda's nonlinear variational procedure. *Comptes Rendus Académie des Sciences Paris, Série IIb*, **320**:563–571, 1995.

[53] P. Suquet. On the effect of small fluctuations in the volume fraction of constituents on the effective properties of composites. *C. R. Mécanique*, **333**:219–226, 2005.

[54] E. Tanné, T. Li, B. Bourdin, J.-J. Marigo, and C. Maurini. Crack nucleation in variational phase-field models of brittle fracture. *Journal of the Mechanics and Physics of Solids*, **110**:80–99, 2018.

[55] P.G. Vincent, P. Suquet, Y. Monerie, and H. Moulinec. Effective flow surface of porous materials with two populations of voids under internal pressure: II. Full-field simulations. *International Journal of Plasticity*, **56**:74–98, 2014.

[56] F. Willot. The power laws of geodesics in some random sets with dilute concentration of inclusions. In J.A. Benediktsson, J. Chanussot, L. Najman, and H. Talbot, editors, *Mathematical Morphology and Its Applications to Signal and Image Processing*, Lecture Notes in Computer Science, pages 535–546. Springer Verlag, New York, 2015.

[57] François Willot. *Localization in random media and its effect on the homogenized behavior of materials*. Habilitation à diriger des recherches, Université Paris Sorbonne, October 2019. https://hal.archives-ouvertes.fr/tel-02412623/file/willotHDR.pdf.

A Laminates

In the case of laminates, the overall surface P^{hom} and the effective surface energy γ^{hom} can be obtained in closed form. For simplicity of notations, we consider here the two-dimensional case (see figure 8), 1 and 2 being respectively the directions parallel and orthogonal to the layers. The specific geometry allows for several different choices of the unit cell, square, rectangle or parallelogram and we will use this flexibility.

A.1 Dual approach (27)

We begin with the analogue of the "static" approach (in the vocabulary of limit analysis). By definition, for any $\boldsymbol{\Sigma}$ in P^{hom} there exists a local "flow" field $\boldsymbol{\sigma}$ satisfying (27). By

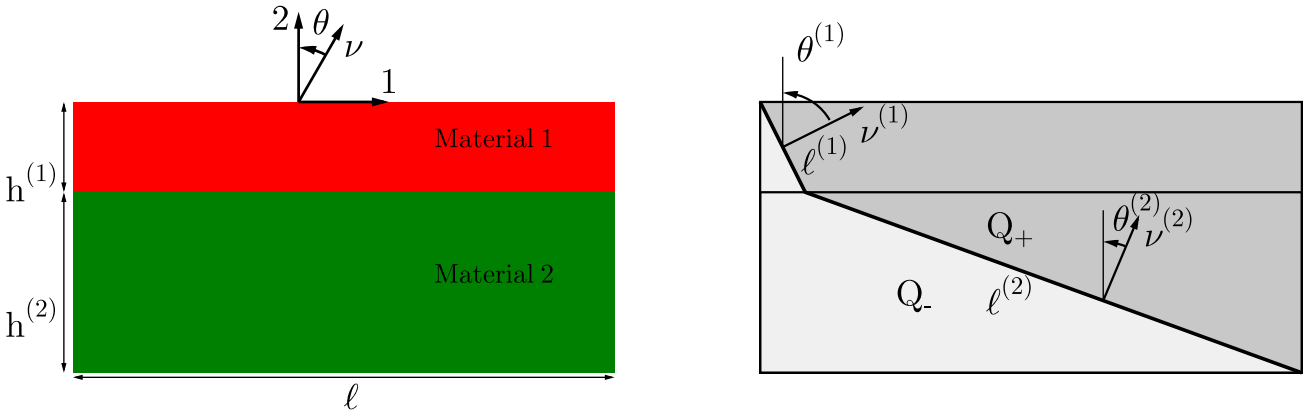

Figure 8: Laminates. unit cell and discontinous field.

translation invariance of the geometry this local field may be assumed to depend only on the variable x_2[7]. The divergence-free constraint implies $\sigma_2 = \Sigma_2$ and $\sigma_1 = \sigma_1(x_2)$. The physical admissibility condition $|\boldsymbol{\sigma}|(\boldsymbol{x}) \leq \gamma(\boldsymbol{x})$ reads as

$$\sigma_1^2 + \sigma_2^2 \leq \gamma^2(x_2), \quad i.e. \quad \sigma_1^2(x_2) \leq \gamma^2(x_2) - \Sigma_2^2,$$

hence the following necessary conditions (recall that $\Sigma_1 = \langle \sigma_1 \rangle$),

$$|\Sigma_2| \leq \inf_{r=1,2} \gamma^{(r)}, \quad |\Sigma_1| = |\langle \sigma_1 \rangle| \leq \langle |\sigma_1| \rangle = c^{(1)} \left((\gamma^{(1)})^2 - \Sigma_2^2 \right)^{1/2} + c^{(2)} \left((\gamma^{(2)})^2 - \Sigma_2^2 \right)^{1/2}, \tag{61}$$

which show that P^{hom} is a subset of the convex set defined by (61). Conversely, let $\boldsymbol{\Sigma}$ be a stress state in $\mathbb{R}^2$ satisfying (61). Then define a local field uniform in each individual phase (r) as

$$\sigma_1^{(r)} = \Sigma_1 \frac{\left((\gamma^{(r)})^2 - \Sigma_2^2 \right)^{1/2}}{c^{(1)} \left((\gamma^{(1)})^2 - \Sigma_2^2 \right)^{1/2} + c^{(2)} \left((\gamma^{(2)})^2 - \Sigma_2^2 \right)^{1/2}}, \quad \sigma_2^{(r)} = \Sigma_2. \tag{62}$$

It is straightforward to check that $\langle \boldsymbol{\sigma} \rangle = \boldsymbol{\Sigma}$ and, with the inequality $(61)_2$ satisfied by Σ_1, that $(\sigma_1^{(r)})^2 \leq (\gamma^{(r)})^2 - \Sigma_2^2$, hence that the constraint $(\sigma_1^{(r)})^2 + (\sigma_2^{(r)})^2 \leq (\gamma^{(r)})^2$ is satisfied in all phases. This shows that P^{hom} coincides with the set (61).

[7] if this is not the case, take the average of the local field $\boldsymbol{\sigma}$ in the x_1 direction. The resulting field will depend on x_2 only and meet all the requirements of (27).

A.2 Primal approach (17)

Continuous fields First, continuous and piecewise affine fields u are considered in (17). The gradient of u is taken to be a constant vector $\boldsymbol{\lambda}^{(r)}$ in each phase. Further restriction on the $\boldsymbol{\lambda}^{(r)}$'s are provided one the one hand by the continuity of the affine field u along the interphase between the two constituents which implies that the discontinuity in $\boldsymbol{\nabla} u$ is normal to the interface, and on the other hand by the average condition $\langle \boldsymbol{\nabla} u \rangle = \boldsymbol{\nu}$. These restrictions lead to the following relations

$$\lambda_1^{(1)} = \lambda_1^{(2)} = \nu_1, \quad c^{(1)}\lambda_2^{(1)} + c^{(2)}\lambda_2^{(2)} = \nu_2, \quad |\boldsymbol{\nabla} u| = \left(\nu_1^2 + (\lambda_2^{(r)})^2\right)^{1/2}. \tag{63}$$

Among the class of piecewise affine trial fields, the optimal one solves the variational problem

$$\begin{array}{c} \mathrm{Inf} \\ \lambda_2^{(1)}, \lambda_2^{(2)} \\ c^{(1)}\lambda_2^{(1)} + c^{(2)}\lambda_2^{(2)} = \nu_2 \end{array} \quad c^{(1)}\gamma^{(1)}\left(\nu_1^2 + (\lambda_2^{(1)})^2\right)^{1/2} + c^{(2)}\gamma^{(2)}\left(\nu_1^2 + (\lambda_2^{(2)})^2\right)^{1/2}. \tag{64}$$

Introducing a Lagrange multiplier Λ for the constraint in (64), the optimality conditions for (64) read as

$$\Lambda = \frac{\gamma^{(r)}\lambda_2^{(r)}}{\left(\nu_1^2 + (\lambda_2^{(r)})^2\right)^{1/2}}, \quad r = 1, 2, \tag{65}$$

from which it is deduced that

$$\left((\gamma^{(r)})^2 - \Lambda^2\right)(\lambda_2^{(r)})^2 = \Lambda^2\nu_1^2.$$

Consequently,

$$\Lambda \leq \begin{array}{c} \mathrm{Inf} \\ r = 1, 2 \end{array} \gamma^{(r)}, \quad \lambda_2^{(r)} = \Lambda\nu_1\left((\gamma^{(r)})^2 - \Lambda^2\right)^{-1/2}, \tag{66}$$

and, finally, the average condition (second relation in (63)) yields, after some re-arrangement, a nonlinear equation for Λ which is solved by any standard means,

$$\Lambda\nu_1\left[c^{(1)}\left((\gamma^{(2)})^2 - \Lambda^2\right)^{1/2} + c^{(2)}\left((\gamma^{(1)})^2 - \Lambda^2\right)^{1/2}\right] = \nu_2\left((\gamma^{(1)})^2 - \Lambda^2\right)^{1/2}\left((\gamma^{(2)})^2 - \Lambda^2\right)^{1/2}. \tag{67}$$

The physical interpretation of the Lagrange multiplier Λ for the average condition in direction 2 is that Λ is the component of the local field $\boldsymbol{\sigma}$ in direction 2, orthogonal to the layers. Once this nonlinear equation is solved for Λ the gradient of u in each phase can be

deduced from (63) and (66) and the effective energy from (64). An alternative expression for γ^{hom} can be derived, which evidences the macroscopic "flow" $\boldsymbol{\Sigma}$ associated with $\boldsymbol{\nu}$

$$\gamma^{\text{hom}}(\boldsymbol{\nu}) = \Sigma_1\nu_1 + \Sigma_2\nu_2, \text{ with } \Sigma_1 = c^{(1)}\left((\gamma^{(1)})^2 - \Lambda^2\right)^{1/2} + c^{(2)}\left((\gamma^{(2)})^2 - \Lambda^2\right)^{1/2}, \quad \Sigma_2 = \Lambda. \tag{68}$$

Discontinuous fields A discontinuous solution to the problem (17) can also be found. This solution u is proportional to the characteristic function of a domain delimited by a crack consisting of two straight lines as shown in figure 8

$$u = 0 \text{ in } Q_-, \quad u = a \text{ in } Q_+,$$

where a is unknown at this stage and determined form the average condition $\langle \boldsymbol{\nabla} u \rangle = \boldsymbol{\nu}$. The length of the crack and its inclination are respectively denoted by $\theta^{(r)}$ and $\ell^{(r)}$ in phase r. For such trial fields, the variational problem (17) is a minimum cut problem which reads as (see notations in figure 8)

$$\begin{array}{c} \text{Inf} \\ \frac{a}{\ell h}\left(\ell^{(1)}\boldsymbol{\nu}^{(1)} + \ell^{(2)}\boldsymbol{\nu}^{(2)}\right) = \boldsymbol{\nu} \end{array} \quad \frac{a}{\ell h}\left(c^{(1)}\gamma^{(1)}\ell^{(1)} + c^{(2)}\gamma^{(2)}\ell^{(2)}\right). \tag{69}$$

After due account of the following geometrical relations

$$\nu_1^{(r)} = \frac{h^{(r)}}{\ell^{(r)}} = \sin\theta^{(r)}, \quad h^{(r)} = c^{(r)}h, \quad \nu_2^{(r)} = \cos\theta^{(r)},$$

the average condition reads as

$$\nu_1 = \frac{a}{\ell h}\left(\ell^{(1)}\sin\theta^{(1)} + \ell^{(2)}\sin\theta^{(2)}\right) = \frac{a}{\ell}, \quad \nu_2 = \frac{a}{\ell h}\left(\ell^{(1)}\cos\theta^{(1)} + \ell^{(2)}\cos\theta^{(2)}\right), \tag{70}$$

so that the variational problem (69) reduces to

$$\begin{array}{c} \text{Inf} \\ \theta^{(1)}, \theta^{(2)} \\ \nu_1\left(c^{(1)}\cot\theta^{(1)} + c^{(2)}\cot\theta^{(2)}\right) = \nu_2 \end{array} \quad \nu_1\left(c^{(1)}\frac{\gamma^{(1)}}{\sin\theta^{(1)}} + c^{(2)}\frac{\gamma^{(2)}}{\sin\theta^{(2)}}\right). \tag{71}$$

Introducing a Lagrange multiplier Λ for the constraint in (71), the optimality conditions for (71) read as

$$\Lambda = \gamma^{(1)}\cos\theta^{(1)} = \gamma^{(2)}\cos\theta^{(2)},$$

and

$$\nu_1\left[c^{(1)}\frac{\Lambda}{\gamma^{(1)}}\left(1 - \left(\frac{\Lambda}{\gamma^{(1)}}\right)^2\right)^{-1/2} + c^{(2)}\frac{\Lambda}{\gamma^{(2)}}\left(1 - \left(\frac{\Lambda}{\gamma^{(2)}}\right)^2\right)^{-1/2}\right] = \nu_2, \tag{72}$$

which after re-arrangment coincides with (67).